Atmospheric Chemistry and Greenhouse Gases

LEAD AUTHOR

D. Schimel

CONTRIBUTING AUTHORS

D. Glover
J. Melack
R. Beer
R. Myneni
Y. Kaufman, C. Justice,
   and MODIS ATBD authors
J. Drummond
   and MOPITT ATBD authors

Chapter 4 Contents

Chapter 4 Contents (cont.)

4.1 Earth Observing System (EOS) program objectives

Any effort to study global change must include quantitative inventories of the forcing agents, specifically atmospheric burdens of greenhouse gases. In addition, the sources and sinks that lead to changing atmospheric concentrations must be known. For simple calculation of radiative forcing, the spatially-resolved concentrations of the relevant gases is sufficient, but neither scientific understanding nor policy is served by such limited data. Scientific understanding requires that the relationships between sources, sinks, and atmospheric concentrations be known in order to: 1) establish whether the causes of the atmospheric changes are explained by anthropogenic or natural causes; and 2) ensure that budgets balance in order to, for example, guarantee that no key processes are missing from our understanding and thus our computational models. Policy formulation further requires that sources and sinks be understood, because, in general, anthropogenic changes to greenhouse gases can only be modified by changing sources or sinks (sources such as fossil-fuel combustion, fertilizer use, sinks by manipulating forest growth, etc.). For the most part, the processes discussed in this chapter can be characterized as "biogeochemical" in that they involve the interaction of biological, geochemical, and photochemical processes.

The EOS program addresses a number of problems in this science area in which space-based measurements are required, or in which synergism between remote sensing and modeling is particularly necessary in order to achieve a global perspective. The EOS program contributes to the study of greenhouse gases and atmospheric chemistry, but is not a stand-alone activity. With our current state of knowledge there are many processes that must be measured in situ, including concentrations of a number of important greenhouse gases, biogeochemical processes in soils or the water column that cannot be remotely observed, and marine and terrestrial stocks of carbon.

Principal foci of the EOS program are using remote sensing to understand and quantify key processes in the global CO_2, CO, CH_4, N_2O, and O_3 budgets, and combining remote observations with theory, modeling, and in situ measurements to develop a tested predictive capability. The EOS program contributes in different ways to understanding the cycles of the different greenhouse gas species. For example, CO_2 and N_2O concentrations cannot be remotely observed in the troposphere with sufficient resolution or accuracy to determine rates of change or spatial distributions. However, many important correlates of CO_2 exchange may be sensed remotely; these include:

- Vegetation index-type measurements (see Chapter 5) that correlate with terrestrial photosynthesis;

- Measurements of terrestrial land cover and land-cover change (see Chapter 5); these influence emissions of many of the trace gases, both directly, as in deforestation and biomass burning, and indirectly. For example, many managed ecosystems have higher N_2O emissions than the corresponding forests;

- Frequency, intensity, and areal extent of biomass burning;

- Ocean-color measurements that relate to marine biological productivity (see Chapter 3);

- Ocean wind stress, which influences CO_2 exchange across the air-sea boundary; and

- Surface climate, which influences CO_2 and N_2O exchange by influencing rates of biological processes.

For the important greenhouse gases, methane and O_3, a different strategy may be employed. In addition to monitoring correlates of methane exchange (such as land cover, inundation, and surface climate), the spatial distribution of methane columns in the atmosphere can be determined by the Measurements of Pollution in the Troposphere (MOPITT) sensor with moderate resolution; methane's oxidation product, CO, can be monitored very accurately (but has many sources in addition to methane related to industrial processes, automobiles, and biomass burning). O_3 is formed in the atmosphere through a complex of photochemical reactions, rather than being emitted from surface sources. Surface sources, biological and anthropogenic, do contribute to O_3 formation by influencing atmospheric NO_x and hydrocarbon concentrations, which form O_3 through a series of reactions. These surface fluxes can be monitored, as they are controlled by many of the same processes that control CO_2, N_2O, and SO_2 exchange. In addition, both O_3 and many of its chemical precursors can be measured in the troposphere directly by the Tropospheric Emission Spectrometer (TES). Key measurements for methane and O_3 include:

- land-cover type and change,
- inundation,
- surface climate,
- methane and CO distributions, and
- O_3 and precursor distributions.

Finally, it must be noted that many processes in the greenhouse gas cycles cannot be monitored directly or by proxy from space and must be quantified globally using models to synthesize multiple data types. Processes such as decomposition or nitrogen turnover that occur in soils and release CO_2, CH_4, and nitrogen trace gases to the atmosphere must be modeled to obtain global estimates (in situ measurements are not feasible except at intensive research sites). The challenge for the EOS program is to incorporate as much global information into such models as possible in order to increase the accuracy of the results.

4.2 Introduction

The study of the cycles of the greenhouse gases includes a huge number of important scientific questions, which include some of the key science questions in the disparate fields of ecology, atmospheric chemistry, oceanography, and human dimensions studies, and are linked to some of the most important environmental management issues of the day. These include not only global climate change, but also acid precipitation (linked to atmospheric NO_x budgets), oxidant damage (largely tropospheric O_3), and habitat destruction (as land-cover change affects the carbon and trace gas cycles and biological diversity [Skole and Tucker 1993]). Key questions addressed by the EOS program are listed below.

4.2.1 Science questions

4.2.1.1   *How does changing land cover/land use affect fluxes of greenhouse gases such as CO_2, methane, and nitrous oxide? How does it affect O_3 precursors from soil (e.g., NO), plant (e.g., biogenic nonmethane hydrocarbons) emissions, and biomass-burning plumes?*

Land-cover change is one of the most potent forces affecting global greenhouse gas changes. In the current carbon budget, fossil-fuel burning and cement production add 5.5 Gt C/yr to the atmosphere (1980s average; Schimel et al. 1995). Land-cover change adds another (although highly uncertain) 1-2 Gt C/yr (Houghton 1995; Table 1 in Schimel et al. 1995). Because land-cover change can in principle be detected using Moderate-Resolution Imaging Spectroradiometer (MODIS) data (Townshend personal communication) and quantified using Landsat or Advanced Spaceborne Thermal Emission and Reflection Radiometer (ASTER) time series (Skole and Tucker 1993), EOS can contribute directly to the estimate of areal changes in land cover. Changes in the carbon content of pre-disturbance and modified landscapes currently must be estimated from in situ data, although radar is a promising alternative for forests.

In addition to influencing CO_2, land-cover changes affect N_2O and NO emissions. In general, forests and undisturbed grasslands have lower rates of nitrogen trace-gas emissions than pastures or croplands (Luizão et al. 1989; Mosier et al. 1991) so land conversion may increase the emissions of these gases. However, emissions decrease with time after conversion (Keller et al. 1993), and so time series of land-cover change are essential to determine time since conversion.

A critical process related to land use is biomass burning. Biomass burning adds CO_2 to the atmosphere as well as a suite of other trace gases. Space-based observations of the extent, frequency, and timing of biomass burning have already proven their value in studies of ecosystem-atmosphere interactions. EOS measurements of biomass burning from MODIS will be a critical feature of future studies of the biogeochemical role of biomass burning.

4.2.1.2   *How does interannual variability in climate affect interannual variability in biogeochemistry?*

Recently, evidence from global observations of CO_2 and O_2 (Ciais et al. 1995; Keeling et al. 1995), CO, CH_4, and N_2O (Dlugokencky et al. 1994), and satellite data (Braswell 1996; Myneni et al. 1996) have indicated that substantial interannual variability in terrestrial ecology and atmospheric chemistry may result from interannual variability in climate, modulated by the internal dynamics and lags resulting from terrestrial ecosystem and oceanic processes (Schimel et al. 1996). Understanding the origins of interannual variability in sources and sinks of CO_2 is important for us to verify our basic understanding of the carbon cycle, and to probe the processes whereby ecosystems and the oceans respond to climate, the latter being crucial for gaining confidence in predic-

tive models. Whereas global observations of CO_2, its isotopes, and O_2 (from global, ground-based observation networks) are the basic tools for observing interannual variability in the carbon budget, remote sensing is the best available method for understanding the geographic distribution of climate anomalies (which, although they may affect the global mean, are not usually distributed homogeneously over the globe) and the spatial response of the oceans and land ecosystems.

4.2.1.3   *How will changing global hydrology and patterns of soil moisture affect fluxes of methane and CO_2 in wetlands?*

Wetlands are a particularly productive environment, yet the processes and fluxes of trace-gas exchange with the atmosphere are inadequately understood and are only beginning to be measured on a global scale. For example, the methane budget is strongly affected by wetland sources, both natural and anthropogenic (Aselmann and Crutzen 1989; Bartlett and Harriss 1993). Consequently, in order to correctly account for methane terms in global biogeochemical models, it is essential to understand the role of wetlands in methane production as well as the effect of changing wetland distribution.

The extent of wetlands is uncertain because there is no clear basis for identification and classification of wetlands on a global scale. In addition, the areal extent of wetlands is being modified as a result of land-use changes, so that once a globally-consistent classification scheme is established, the areal distribution must be monitored and recompiled. New data are becoming available from remote sensing that provide a global perspective on wetland distribution and classification, but these are not yet reconciled with ground-based ecological and hydrological data.

There have been several remote-sensing studies on characterizing various types of wetlands at differing scales using airborne and spaceborne systems (Hess et al. 1990, 1995; Pope et al. 1992, 1994; Morrissey et al. 1994). Most of these studies have been at a local scale using airborne systems. Current optical and microwave algorithms need to be evaluated and implemented for generating new, improved regional and global data sets on wetland extent and seasonality.

4.2.1.4   *What is the spatial distribution of tropospheric O_3? How do changing surface fluxes of precursor species affect the tropospheric O_3 budget?*

Tropospheric ozone is a key species in atmospheric chemistry and a critical link between atmospheric chemistry and the Earth system. Ozone is produced in the atmosphere by photochemical processes and is derived from precursor gases that have their origin in stratospheric chemistry, the biosphere, oceans, and industrial processes. Changes to the tropospheric ozone budget result from changing sources of precursors arising from fossil-fuel burning, biomass burning, and, possibly, changing biogenic sources in soils and vegetation. Ozone is a key species in the troposphere because it is a potent greenhouse gas in the mid and upper troposphere, and damaging to vegetation and human health at high concentrations near the Earth's surface. Because its distributions in space and time are very heterogeneous, reflecting its short lifetime, global spatial data on its distribution are key to understanding both how global tropospheric chemistry is changing, and how those changes may affect climate and the biosphere. The effects of ozone on UV radiation are also very important and are dealt with elsewhere (see Chapter 7).

4.2.1.5   *What is the vertical distribution of tropospheric O_3? What controls this distribution and how is it affected by stratosphere-troposphere exchange, the changing geography of surface sources of precursors, and by anthropogenic sources (aircraft) in the free troposphere?*

Knowledge of the vertical distribution of ozone is critical. The vertical profile of ozone from the mid-stratosphere to the surface influences the integrated radiative effect of ozone, and, hence, its effects on climate. Since large increases in surface concentrations can occur in areas polluted by automobiles, industry, and biomass burning, information on high surface levels is likewise critical. Understanding how the vertical profile of ozone may change in the future requires knowledge of how the vertical profile could change as the geography of sources changes, if atmospheric convection and mixing change (affecting the rate in which ozone and its precursors are mixed through the troposphere), and with the introduction of anthropogenic sources (e.g., subsonic aircraft). Because understanding the vertical distribution of ozone requires understanding of sources, subsequent chemistry, transport, stratosphere-troposphere exchange, and sinks, accurate predictive models will be extremely difficult to develop and evaluate without strong constraints from global observations.

4.2.1.6   *How do physical, chemical, and biological processes interact to control ocean carbon uptake?*

By continually exchanging heat and greenhouse gases with the atmosphere, the global ocean plays an important role in the regulation of the Earth's climate. The ocean alone

contains about 50 times more carbon than the atmosphere and, paradoxically, because of its large buffering capacity, the ocean has the potential (if instantaneously ventilated to the atmosphere) to absorb approximately 6000 Gt of additional CO_2. This very large number is misleading, however, as it assumes all of the ocean can be brought into contact with the atmosphere at once. In reality, only the surface waters of the ocean are ventilated with the atmosphere, and, because this is a reversible chemical reaction, only a small fraction of this CO_2 would be neutralized by the time a new equilibrium is reached. Much later, on the order of thousands of years, this added CO_2 will react with the $CaCO_3$ in the ocean, in effect recharging the surface water's neutralizing capacity. In the end, it's not the distribution of CO_2 in the ocean but rather the distribution of the ocean's alkalinity that drives this absorption.

The kinetics of CO_2 gas transfer across the ocean-atmosphere interface is slow, on the order of a year. This rate is slower than processes such as the biological uptake of carbon that significantly affects seasonal partial pressure of CO_2 (pCO_2) in surface seawater over time scales of days to months. Consequently, the process of CO_2 gas exchange between the ocean and atmosphere is controlled by the complex interactions of biological activities throughout the water column, the chemical buffering capacity of the ocean for CO_2, and ocean circulation dynamics (see Sections 4.1.1.3, 4.2.4.2, 4.2.4.3, and 4.2.4.5). The relative importance of these processes varies both temporally and spatially. New data from atmospheric $^{13}CO_2$ and O_2 measurements provide a new, globally-integrated view of these processes, but little insight into how and where the processes are occurring. Atmospheric data suggest that only approximately 55% of the anthropogenic CO_2 gas injected into the atmosphere remains there. The remaining and rather variable 45% is taken up by both the ocean and the terrestrial biosphere. What controls this partitioning and its changes in time?

4.3 EOS data products and synthetic analyses

4.3.1 Introduction

This section addresses the specific scientific activities, data products, and algorithms currently in progress within the EOS program. This discussion will describe the specific "deliverables" as we now envision them. The deliverables are grouped under the subheadings: Carbon Cycle, Methane, Nitrous Oxide, and Atmospheric Chemistry and Ozone, but in fact there is considerable synergism between the measurements and models for the different trace gases. In Section 4.4, the space-based observations and algorithms that support these scientific deliverables are described in more detail.

4.3.2 The carbon cycle

The major fluxes of the carbon cycle on interannual-to-centennial time scales are illustrated in Figure 4.1. This figure does not show some of the millennial-to-longer processes such as calcite dissolution, carbonate mineral formation, and other rock-cycle processes. The processes include background fluxes, characteristic of the undisturbed biosphere, such as the nearly balanced air-sea and terrestrial primary production-respiration exchanges of ~90 and ~60 Gt C/yr, respectively. The figure also illustrates so-called perturbation fluxes that result directly or indirectly from anthropogenic activity. These include fos-

sil fuel plus cement production, fluxes from land-use change, and the imbalances in air-sea exchange (~2 Gt C/yr) and in net primary production (NPP)-respiration exchange (~1.4 Gt C/yr). Components of the EOS program address measurement of both the perturbation fluxes (which are the terms usually referred to as "the global carbon budget") and the magnitude or at least the variability in some of the background fluxes.

4.3.2.1 Quantify land-cover change and convert to carbon changes

Land-cover change is one of the fundamental factors perturbing the global carbon cycle. In the most recent Intergovernmental Panel on Climate Change (IPCC) assessment, conversion of forests to managed systems (pastures and cropland) in the tropics was estimated to release 1.6 (±1) Gt C/yr to the atmosphere. Conversely, the regrowth of midlatitude forests harvested a half-century to a century ago may be absorbing 0.5-1.0 Gt C/yr. (The values given are average rates for the 1980s.) Satellite and other evidence suggests that land conversion may be quite variable from one year to the next. Current efforts in the EOS project and within the Earth Science Enterprise (ESE) (carried out by IDS and Pathfinder teams) are using Landsat, Systeme pour l'Observation de

FIGURE 4.1
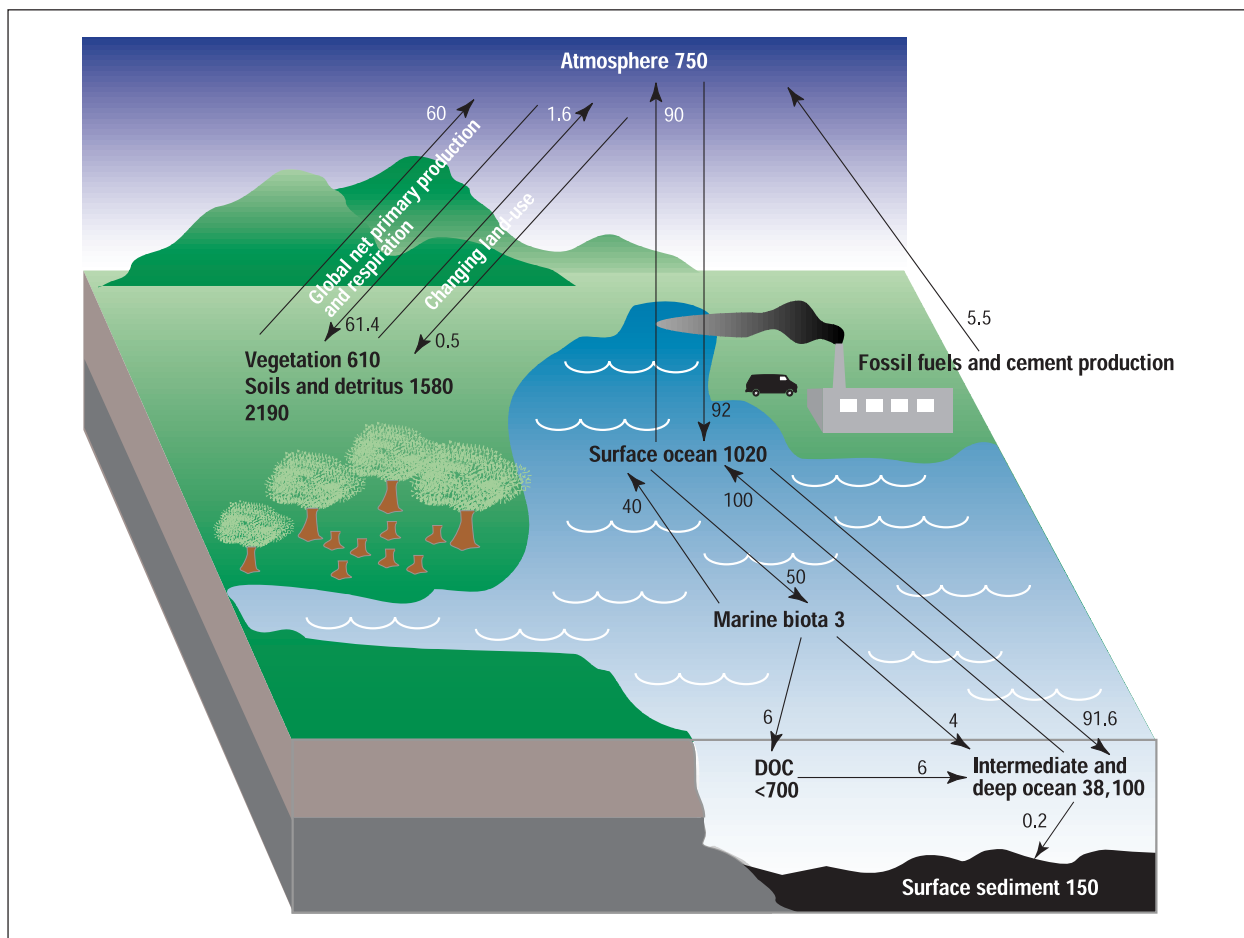
The global carbon cycle, showing the reservoirs (in Gt C) and fluxes (Gt C/yr) relevant to the anthropogenic perturbation as annual averages over the period 1980-1989 *(Siegenthaler and Sarmiento 1993; Potter et al. 1993; Eswaran et al. 1993).* **The component cycles are simplified and subject to considerable uncertainty. In addition, this figure presents average values. The riverine flux, particularly the anthropogenic portion, is currently very poorly quantified and so is not shown. Evidence is accumulating that many of the key fluxes can fluctuate significantly from year to year** *(terrestrial sinks and sources: INPE 1992; Ciais et al. 1995; export from the marine biota: Wong et al. 1993).* **In contrast to the static view conveyed by figures such as this one, the carbon system is clearly dynamic and coupled to the climate system on seasonal, interannual, and decadal time scales** *(Schimel and Sulzman 1995).*

la Terre (SPOT), Japanese Earth Remote-sensing Satellite (JERS)-OPS, and European Remote-Sensing Satellite (ERS-1) data to quantify rates of land-cover change in selected case-study regions. (The Brazilian Amazon, Thailand, Cambodia, Laos, Vietnam, several West African regions, and Costa Rica are currently under study by a range of investigators.) In addition to identifying primary land conversion, successful efforts are underway to estimate regrowth in secondary forest, a key factor in carbon balances. Future EOS efforts will take advantage of the ASTER, Landsat, and international sensors to continue to build an increasingly global database of high-resolution analyses of land-cover change. These high-resolution

data are also being used to calibrate and validate retrievals of land cover and land-cover change using lower-resolution sensors (such as AVHRR), an effort that will continue with MODIS.

Additionally, MODIS will provide estimates of the timing, frequency, and extent of biomass burning. These retrievals utilize a special MODIS channel, with the appropriate dynamic range not to saturate over biomass-burning sources (http://eospso.gsfc.nasa.gov/atbd/modis/atbdmod15.html). This retrieval, coupled with in situ estimates of biomass density and emission factors (CO_2 released/unit biomass consumed) allows spatially-resolved estimates of the contribution of biomass burning

to atmospheric CO_2. Similar algorithms are used for other trace gases.

4.3.2.2   Monitor correlates of terrestrial CO_2 exchange through photosynthesis and respiration; use models to quantify variability and trends in carbon storage

4.3.2.2.1   EOS LAI and FAPAR products

The importance of vegetation in studies of global climate and biogeochemical cycles is now well recognized (Sellers and Schimel 1993). This is especially the case with respect to carbon, as the exchange of carbon between plants and the ambient air involves vast quantities of gaseous carbon dioxide, an important greenhouse gas. In order to estimate carbon fixation by terrestrial vegetation and to prescribe the land surface accurately in global climate models, variables descriptive of surface assimilation area, radiation absorption, plant physiology, and climatology are required. The consensus is that such multi-temporal global data sets can be regularly obtained only from remote sensing. Therefore, several of the instruments scheduled for EOS have land-surface-parameter estimation as major deliverables (Asrar and Greenstone 1995).

Two key variables required in primary production and global climate studies are leaf-area index (LAI) and fraction of photosynthetically-active radiation (0.4 - 0.7 μm) absorbed by the vegetation (FAPAR) (Sellers et al. 1986; Ruimy et al. 1994). Leaf-area index is generally defined as one-sided green-leaf area per unit ground area in broadleaf canopies, and variously (projected or total) in needle canopies. Unlike LAI, FAPAR exhibits diurnal variation. Its use in models with time steps longer than a day requires appropriate time resolution. It has a spatial resolution of 1.1 km. There are two algorithms to derive LAI and FAPAR. The first is a Normalized Difference Vegetation Index (NDVI)-based approach, supported by substantial theoretical and empirical evidence. The second algorithm to derive accurate estimates of LAI and FAPAR is a look-up-table-based approach that is capable of exploiting the spectral nature of MODIS measurements and the angular nature of Multi-Angle Image Scanning Radiometer (MISR) measurements. A comprehensive three-dimensional radiative transfer model for vegetated surfaces is utilized by both algorithms to connect remote observations to surface variables of interest in a manner that is consistent with the spatial scale of the observations. The algorithms require a land-cover classification that is compatible with the radiative-transfer model used in their derivation. Global land covers can be classified into six biome types depending on the canopy structure:

grasslands/cereal crops, shrublands, broadleaf crops, savannas, broadleaf forests, and needleleaf forests. Further details on theoretical aspects, implementation, and accuracy can be found in Myneni et al. (1996).

4.3.2.2.2 Interannual variations in atmospheric CO_2

A measurable link between atmospheric CO_2 drawdown by vegetation and NDVI dynamics was demonstrated by Tucker et al. (1986). Interannual variations in observed atmospheric CO_2 and inferred biospheric carbon exchange since 1980 were discussed recently by Keeling et al. (1995). The biosphere was found to be a source of carbon during the warm events and a sink during cold events. The atmospheric CO_2 anomaly, with respect to a 20-year baseline period (1959-1979), increased from 1980 to late 1988 and has decreased. The global NDVI anomaly, which is indicative of photosynthetic carbon fixation by plants, was mostly negative during the period of increasing atmospheric CO_2 anomaly, and, starting from late 1988 it was positive until mid-1991, when the eruption of Mount Pinatubo corrupted the satellite data (private communication from R. B. Myneni 1996).

While the 1980s experienced well-defined sea-surface temperature (SST) oscillation events both in the equatorial Pacific (Woodruff et al. 1993) and tropical Atlantic (Philander 1986), the situation during the 1990-1995 time period was different. There were three weak warmings in the equatorial Pacific begining from early 1991 onwards. The strong co-variation between biospheric carbon exchange and NINO3 index observed in the 1980s appears weakened from early 1991 onwards. The decrease in atmospheric CO_2 anomaly from the time of the Mount Pinatubo eruption in mid 1991 until late 1993 was uncharacteristically sharp (Keeling et al. 1995). Although air temperatures decreased following the Mount Pinatubo eruption, the global anomaly is still high, about 0.3°C (Jones et al. 1994), and 1995 was the warmest year so far (Anonymous 1996).

In a recent study, Keeling et al. (1996) reported that the amplitude of the seasonal CO_2 cycle in the Northern Hemisphere increased on an average by about 30% since the early 1960s, thus indicating increased Northern Hemisphere biospheric activity. Moreover, the midpoint in atmospheric CO_2 drawdown between spring and summer was found to be advanced by about 7 days, which they interpret as an indication of a longer growing season. This important result has lately been confirmed from analysis of satellite-derived NDVI data (private communication from R. B. Myneni 1996). Thus, both the radiometric data and the atmospheric CO_2 record seem to indicate that the global carbon cycle has responded to

interannual fluctuations in temperature, which may be small at the global scale but potentially significant at the regional scale.

4.3.2.2.3 ENSO & NDVI

SST in the tropical Pacific is coupled with atmospheric phenomena such as pressure fields, wind fields, large-scale convection of moist air from the ocean to the atmosphere, oceanic and continental rainfall, and other atmospheric processes (Philander 1990). Large-scale SST variations on the order of 2-3°C in the tropical Pacific Ocean are reported to have dramatically perturbed global precipitation and temperature patterns through displacement of major rain-producing convergence zones in the tropics and atmospheric circulation changes, causing torrential rains in some areas and severe droughts in others, with associated crop failures, forest fires, mud slides, floods, and other natural disasters (Glantz et al. 1991).

Several workers have compared surface precipitation records with El Niño Southern Oscillation (ENSO)-cycle SST anomalies, identifying areas where precipitation anomalies were correlated with tropical Pacific SST anomalies (McBride and Nicholls 1983; Ropelewski and Halpert 1987, 1989). Point rainfall frequently does not adequately represent areal rainfall, especially in semi-arid tropical regions where rainfall is often erratically distributed. Thus, accurate estimates of the geographical extent of SST-linked precipitation anomalies have been hampered in many areas. Satellite-derived NDVI data, which several studies have shown to be highly correlated with arid and semi-arid rainfall (Tucker et al. 1991), have been used to correlate tropical Pacific SST anomalies from the NINO3 region (5° S to 5° N latitude and 90° W to 150° W longitude) in order to delineate anomalous rainfall areas through direct measurement of vegetation amount and condition in a spatially-continuous manner for arid and semi-arid areas.

The 1980s experienced well-defined alternating ENSO warm and cold events (Philander 1990). It was found that large areas (between 0.5 and 1.5 million km^2) in semi-arid regions experienced rainfall anomalies that were directly correlated to SST anomalies in the equatorial Pacific. Although the warm events of the ENSO cycle were associated with decreased rainfall and the cold events with increased rainfall, this pattern was not always consistent, at least during the 1982-1990 time period. For instance, southeastern South America encompassing regions in southern Brazil, northern Argentina, Paraguay, and Uruguay experienced a strong drought during the 1988-89 cold event of the ENSO cycle (Myneni et al. 1996). This analysis confirmed the disruptive effects of large-scale SST anomalies on regional-scale precipitation patterns and, therefore, vegetation in arid and semi-arid regions of Africa, Australia, and South America for the time period of 1982-1990.

4.3.2.2.4 Interannual variations in Gross Primary Production (GPP)

GPP denotes the amount of carbon photosynthesized by plants. Some of this carbon is respired, while the rest is invested in plant growth. Seasonal and interannual variations in GPP of terrestrial vegetation are therefore of considerable interest. Monthly GPP estimated from monthly mean global green-leaf area and photosynthetically-active radiation derived from observations made from several geostationary and polar orbiting satellites for the years 1982 through 1990 were recently investigated by Myneni et al. (1995).

Interannual variations in GPP, of the order of 1.6 Pg C, were reported by Myneni et al. (1995). Interestingly, this is in good agreement with results on the interannual variability of atmospheric CO_2 increase (Conway et al. 1994). The largest year-to-year changes in atmospheric CO_2 increase, of the order 2-3 Pg C, occurred during the 1982-1983 and 1986-1987 El Niño/Southern Oscillation events. Similar large year-to-year changes in GPP were also observed (4.3 and 2.3 Pg C, respectively). In fact, the evolution of monthly GPP anomalies was reported to be similar to the atmospheric CO_2 growth rate during 1982-1990. That is, periods of increasing atmospheric CO_2 were coincident with periods of higher-than-average biospheric GPP and vice versa. This was observed both globally and for the 30°-90° N latitudinal band, but not for other latitudes 0-30° N, 0-30° S, and 30°-90° S. If NPP is assumed to be a constant fraction of GPP, then heterotrophic respiration and biospheric NPP must respond similarly but disproportionately to climate in order to match the observed atmospheric CO_2 growth rate (disregarding small variations in net oceanic exchange). This inability of heterotrophic respiration to balance biospheric NPP could be the likely mechanism by which the so-called missing carbon (Tans et al. 1990) is being sequestered into soils, ultimately, via biospheric net fixation. This needs to be confirmed, although some evidence of carbon sequestration in tropical soils has recently been reported (Fisher et al. 1994).

4.3.2.3 *Monitor correlates of oceanic CO_2 change on short time scales (pCO_2 proxy and wind stress)*

The atmospheric signal of CO_2 change should now be large in the ocean, hypothesized to correspond to approximately 45 µmol/kg total inorganic carbon in the modern

surface ocean. However, traditional direct oceanic observations are incomplete and cannot unambiguously confirm this hypothesis. The seasonal range in pCO_2 due to biological activity alone can be as large as 200 µatm (corresponding to approximately half the anthropogenic signal). Other confounding changes to the CO_2 concentration of the upper ocean, such as thermal effects, help mask the other half of this signal. We will need answers to pressing global-change problems before this portion of the carbon cycle can be sorted out through more-traditional means.

Thus, continuous, near-synoptic measurements of CO_2-influencing processes can be a boon to the Earth system science of the global carbon budget. EOS data will help identify, on a global scale, areas of high biological activity (via ocean-color data, see Section 4.3.2.5) and of intense mixing and ocean-atmosphere CO_2 flux due to wind stress (via altimetry and scatterometry, see Sections 4.3.1.1, 4.3.2.3, and 4.3.4.6). Data assimilation of altimetry will improve models of ocean circulation, especially those of the upper ocean where ocean-atmosphere interactions take place (see Section 4.3.1.2). By combining our current knowledge (largely physical) with our EOS-enhanced knowledge (largely biological) we will be able to monitor the behavior of CO_2 in the surface waters of the ocean well enough to separate natural from anthropogenic signals (see relevant sections in Chapter 2).

4.3.2.4   Integrate the above into global synthetic analyses

Understanding the global carbon cycle requires the integration of terrestrial, aquatic, and marine exchanges to produce a global budget. It also requires information on the anthropogenic fluxes of CO_2 from fossil-fuel combustion and cement manufacture (data available through the Carbon Dioxide Information and Analysis Center [CDIAC] and the Socioeconomic Data and Applications Center [SEDAC]). Within the EOS program, efforts are being made to develop and intercompare models of the component systems (ocean models and terrestrial biogeochemical models) and to integrate them via atmospheric transport models. Several groups within EOS and in collaboration with EOS have developed and applied models of the carbon cycle. These models have been used in specific case-study modes for intercomparison and validation (Figure 4.2; VEMAP members 1995; Schimel et al. 1996), and in inverse calculations, where the best fit between atmospheric observations and modeled spatial distributions of fluxes is sought using mathematical techniques (Figure 4.3; Ciais et al. 1995; Denning et al. 1995). As more information becomes available, both from atmospheric observations and from space, these integrated

inverse and forward models will become a more-important part of the EOS program.

4.3.3   Methane

After CO_2, changing methane is the second largest perturbation of the radiative forcing of the atmosphere (see Chapter 8 for a discussion of the countervailing effects of sulfur gases). Methane is produced via a number of pathways, mostly involving biological processes in reducing (low oxygen) environments. Methane is produced when heterotrophic bacteria have insufficient O_2 to use as electron acceptors in metabolism, and insufficient SO_4 to use sulfur compounds to fuel energy metabolism. Key methanogenic environments include natural wetlands, paddy rice cultivation, the rumens (stomachs) of cattle and other ruminant wild and domestic animals, and landfills. At a process level, methane production in wetlands and rice-growing regions is reasonably well-understood. In these systems, methane production occurs largely during seasons of inundation, where soils are sufficiently flooded that oxygen, which diffuses slowly in water, becomes limiting to microbial metabolism (Paul and Clark 1989). Methane is produced predominantly from recently produced carbon, and so methane production increases, in general, as primary productivity increases (Dacey and Klug 1979; Valentine et al. 1994). Large methane fluxes occur in regions of high primary productivity and prolonged inundation. Thus, intensively managed rice fields may have extremely high rates of methanogenesis, as may some natural wetlands. It is important to note that in our present state of knowledge, the methane budget is not balanced: known sources do not equal known sinks, although the difference is within the uncertainty of the estimates (Prather et al. 1995). This is of concern as it adds uncertainty to estimates of methane's lifetime and leaves open the possibility of an important but unknown process. Thus, spatial analyses of methane dynamics remain of considerable importance.

Also of importance is the fact that methane is oxidized to CO_2 in aerobic soils, although the dominant sink for methane is photochemical oxidation in the atmosphere. In aerobic soils, where oxygen is plentiful, methane oxidation typically occurs at intermediate soil-moisture levels (Mosier et al. 1991). Rates of methane oxidation are typically reduced in derived (pastures and cropland) as compared to native ecosystems (Mosier et al. 1991; Keller et al. 1993). Furthermore, the use of nitrogen fertilizer seems to inhibit methane oxidation (Mosier et al. 1991).

Key EOS products include wetland hydrology (extent and duration of inundation) and land cover and productivity in methanogenic regions and in areas of methane oxidation (using satellite data and models: see
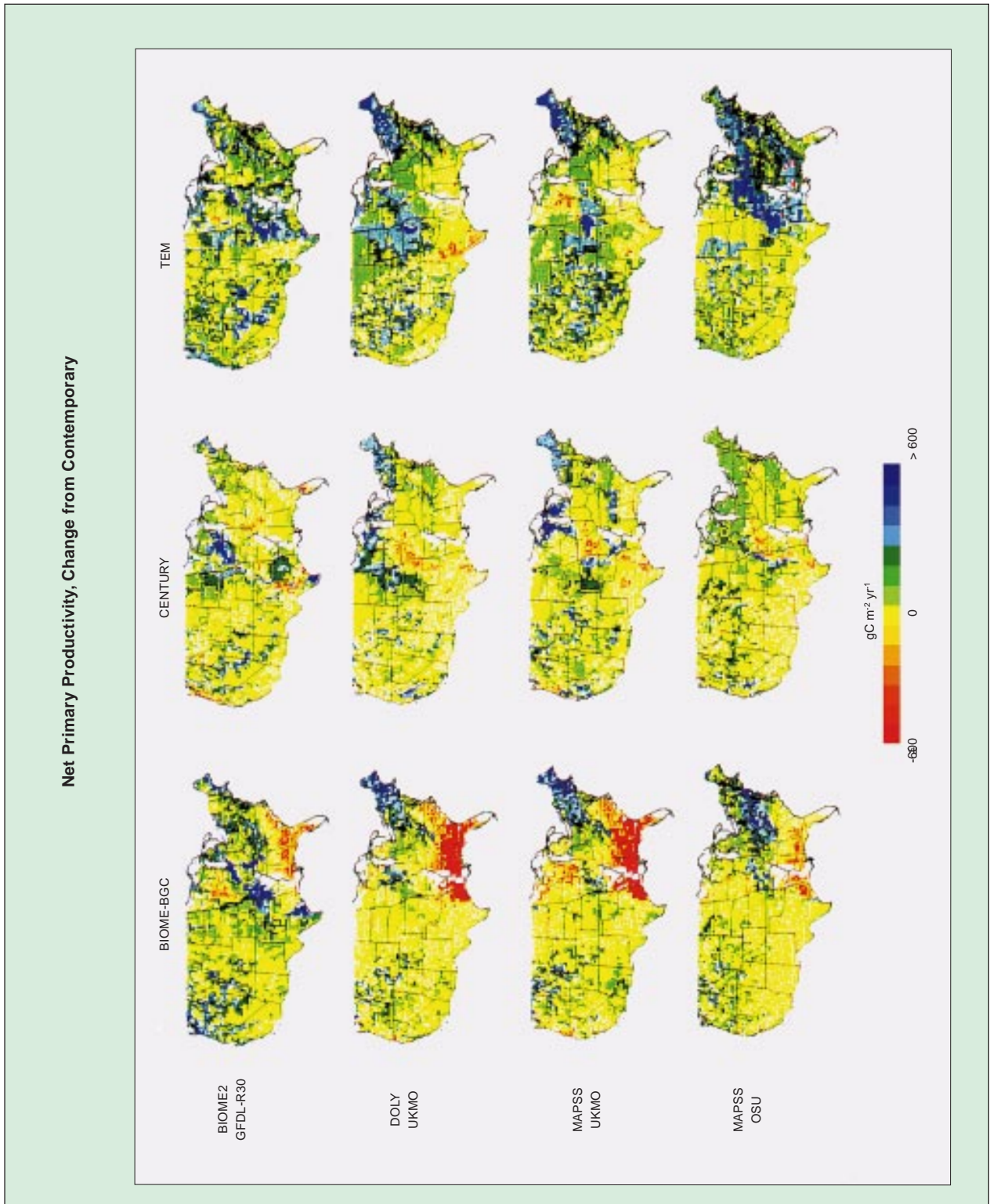
Comparison of changes in annual net primary productivity (NPP) estimates when biogeochemistry models (BIOME-BGC, CENTURY, TEM) are run with the vegetation distributions of the biogeography models (BIOME2, DOLY, MAPSS) for particular climate scenarios (GFDL-R30, UKMO, OSU) *(VEMAP 1995)*
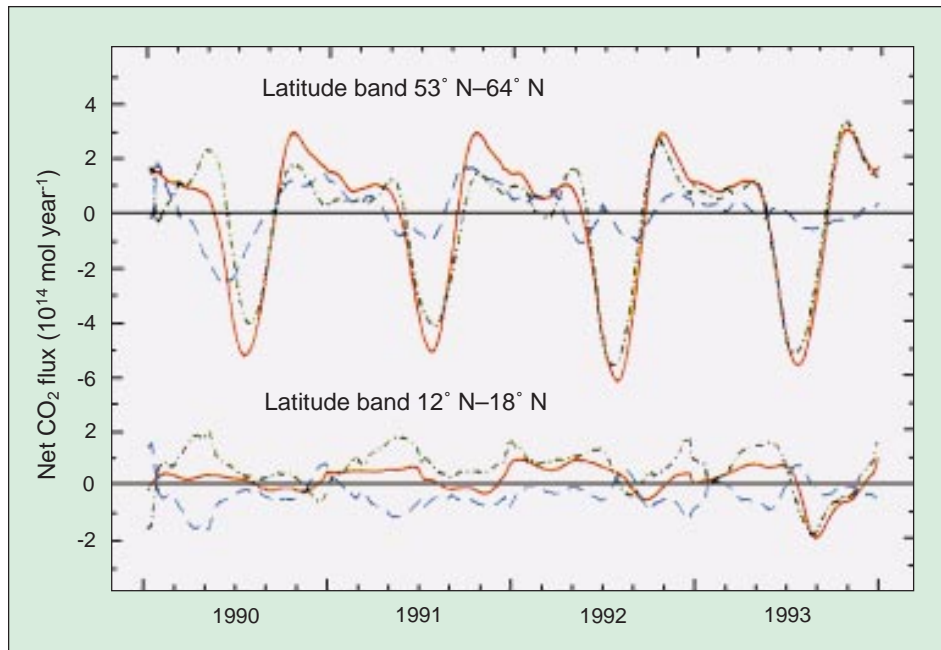
Ocean and land partitioning of CO_2 fluxes as a function of time. Latitude bands in the tropics and at northern midlatitudes are shown as examples. At northern midlatitudes, the lower values for net uptake during 1990 and 1991 are artifacts of the sparser isotopic measurements in those years. When constrained with sufficient data, the seasonality of carbon uptake in the tropics is clearly terrestrial. We note that the mirroring effect of the terrestrial biospheric and oceanic fluxes for the tropical zone may be indicative of a problem with the isotopic data. The solid line shows the annual mean net flux of CO_2 without the contribution of fossil-fuel emissions. The dashed line is the net exchange of CO_2 with the oceans. The dash-dot line is the net exchange on land *(Ciais et al. 1995).*

vanced airborne SAR systems have been developed, and five spaceborne SAR systems—ERS-1 and 2, JERS-1, Radarsat, and Shuttle Imaging Radar-C (SIR-C)/X-SAR—have been deployed. Additional spaceborne SARs are likely to be launched throughout the remainder of this decade and into the next.

For most scientific questions involving wetlands, it is necessary to distinguish not only flooded vs. non-flooded areas, but herbaceous vs. woody vegetation. Delineation of both flooding status and vegetation, with accuracies greater than 90% for all categories, has been demonstrated using multi-frequency, polarimetric SAR data sets for wetlands in the southeastern United States (Jet Propulsion Laboratory Airborne Synthetic Aperature Radar [JPL AIRSAR]) and the central Amazon (SIR-C) (Melack et al. 1994; Hess et al. 1995). Based on these studies, which included extensive field verification, and on modeling studies (Wang et al. 1995), the following generalizations can be made:

1) While C-band is adequate for distinguishing flooding in marshes, it can reliably detect forest inundation only where stem densities are low. L-band is required for flood detection in most floodplain forests.

2) Horizontal, horizontal polarization (HH) is the best polarization for flood detection in both forests and marshes.

3) Two wavelengths are required to reliably separate woody from herbaceous vegetation. The greater the contrast in wavelengths, the better the separation: C and L provide good results, and C and P provide better results; the combination of X and L requires further study. Although L-band HH (LHH) alone can readily distinguish between woody and non-woody vegeta-

MODIS ATBD 17; http://eospso.gsfc.nasa.gov/atbd/modis/atbdmod17new.html), biomass burning, and direct retrievals of methane. These products can be used in models of atmospheric chemistry to constrain estimates of surface emissions based on atmospheric methane budgets.

4.3.3.1   Monitor land-use/land-cover correlates: wetland extent and hydrology, including natural wetlands, rice cultivation, and biomass burning

4.3.3.2   Delineation of wetland inundation and vegetative cover with microwave remote sensing

Characterization of the areal and temporal extent of wetlands would greatly extend our understanding of trace-gas exchange from these ecosystems and of their significance to global processes. The availability of Synthetic Aperture Radar (SAR) data from airborne and satellite platforms has provided a unique opportunity to study dynamic wetland processes related to biogenic trace-gas exchange by providing information on the type and distribution of wetlands and temporal distribution of inundation. During the past five years a number of ad-

tion on non-flooded sites, the situation is more complex where flooding is present, because flooding can increase LHH backscattering from herbaceous vegetation to values nearly identical to those from unflooded forest.

The ability to penetrate the extensive cloud cover and to detect standing water beneath vegetation canopies is unique to SAR (Hess et al. 1990). SAR has proven useful in delineating levels of inundation; backscatter from ERS-1 SAR acquired over Barrow, Alaska, in 1991, is strongly related to the position of the local water table and thus to methane exchange rates (Morrissey et al. 1994). The capability to differentiate wetland source areas and non-wetlands with SAR is further enhanced by the availability of time-series data. While species composition per se usually cannot be detected with SAR, plant communities often can be detected due to differences in vegetation height, density, or architecture (Pope et al. 1994).

A global record of passive microwave observations from satellites is available from 1979 to the present. The Scanning Multichannel Microwave Radiometer (SMMR) was operated on board the Nimbus-7 satellite from 1979 to 1987, with global coverage every six days. The Special Sensor Microwave/Imager (SSM/I) replaced SMMR in 1987 and continues today with three-day global coverage. These microwave emission measurements include both vertical and horizontal polarizations and four frequencies. For wetland studies, the two highest frequencies, 37 GHz (SMMR and SSM/I) and 85.5 GHz (SSM/I only), are the most useful because they offer the best spatial resolution (ca. 30 and 15 km, respectively). Passive microwave emission measurements are expressed as brightness temperatures in kelvins, and the difference between the two polarizations may be referred to as DT. The principal advantages of the passive microwave observations are their frequent global coverage and their ability to reveal certain characteristics of the land surface beneath cloud cover and vegetation. The coarse spatial resolution may be an advantage for global studies because it reduces the data volume, but it is often a limitation for studies of specific sites.

SMMR observations of the 37 GHz DT have been analyzed to determine spatial and temporal patterns of inundation in the extensive floodplains of the Amazon River (Sippel et al. 1994) and the Pantanal wetland (Hamilton et al. 1996) of South America. The utility of passive microwave remote sensing to monitor inundation in other wetlands of the world has yet to be investigated. The coarse spatial resolution limits the application of the technique to large wetlands, or to regions where the cu-

mulative area of smaller wetlands comprises a significant proportion of the landscape. Surface roughness, exposed soil and rock, seasonal vegetation changes, and seasonal snow cover can affect the DT (Choudhury 1989), and these factors may have to be accounted for to quantify the variability in flooded areas using microwave emission.

There have been many investigations of the potential use of passive microwave remote sensing to quantify surface soil moisture (Jackson 1993). Soil-moisture studies have focused on arid and semi-arid regions where bare soils dominate, or in agricultural areas. Jackson and Schmugge (1991) discuss the effects of vegetation on the microwave emission from soils and conclude that there is little chance of reliably estimating soil moisture under forest or shrub canopies, which attenuate the emission from the soil surface. In addition, the lowest frequency available for satellite data is 19.4 GHz, where emission represents less than 1 cm of soil depth, and the satellite measurements have a spatial resolution of about 50 km.

4.3.4 Nitrous and nitric oxide

Nitrous oxide (N_2O) is an important greenhouse gas, with an atmospheric lifetime longer than 100 years. It is produced by microbial processes in soils and increases with intensified land use, especially as a result of fertilization. Nitric oxide (NO), a short-lived, chemically-active species is produced by these same microbial processes, but is not a greenhouse gas; however, increasing levels of NO in the atmosphere lead to higher production of atmospheric O_3, an important greenhouse gas. Nitrous oxide is increasing in the atmosphere (although its annual rate of growth is low), and soil NO emissions may well be increasing. Changes to the atmospheric N_2O content can be measured directly, but changes in NO are hard to detect globally, because NO's short atmospheric lifetime means that atmospheric concentrations are low and spatial variability is extremely high. However, the NO_x family of compounds (NO, NO_2, HNO_3, . . .) can be measured from space, complementing surface observations, which have lower spatial resolution although potentially higher temporal resolution than from space.

4.3.4.1 Monitor terrestrial correlates processes that influence N_2O and NO emissions

This task parallels the tasks described for the carbon cycle. Conversion of forests to other uses such as pasture or cropland will for a time increase nitrogen trace gas emissions. The basic science requirement here is to provide periodic assessments of land cover along with, at a minimum, indicators of regions that are undergoing rapid change (from change-detection algorithms). Relatively frequent assessment of land-cover change will be necessary in areas of

rapid land-cover change because of the dependence of trace-gas emissions on time since disturbance. Both NO and N_2O emissions have been shown to depend upon time since conversion from forest to pasture (Keller et al. 1993), and may depend upon time since conversion from grassland to cropland.

4.3.4.2   Monitor soil moisture

Soil moisture is a key control over nitrogen trace-gas fluxes. Soil moisture content affects both the species of nitrogenous trace gas emitted, and the overall rate of nitrogen trace-gas emissions (Parton et al. 1988). In general, overall NO and N_2O emissions increase with increasing soil moisture up to a maximum level related to the fraction of overall soil volume filled with water (water-filled pore space [WFPS]) (Firestone and Davidson 1989; Davidson 1992). Above the WFPS threshold, emissions of the inert gas N_2 may continue to increase, but emissions of reactive species may decline. In addition, there is evidence that emissions of NO occur in "pulses" immediately following each rainstorm in more-arid conditions (Yienger and Levy 1995), so knowledge of event frequency is itself a useful variable. Whereas there are severe technical problems with remotely measuring soil moisture (a) under dense vegetation and (b) below a few centimeters depth, there are several potential EOS contributions of space-based measurements. First, there is some promise that microwave surface "wetness" retrievals may eventually be correlated with more-quantitative measures of soil moisture. This is hopeful for trace gases as, in many ecosystems, most N metabolism occurs near the soil surface (Schimel et al. 1986). Second, soil-moisture retrievals from 4-Dimensional Data Assimilation (4DDA) may be useful. This latter possibility is crucial, as constrained but physically-based estimates of soil moisture linked to an integrated hydrological calculation could result in critical improvements in global soil-moisture estimates. These techniques are most hopeful for the upper soil layers, where water content is most tightly coupled to the atmosphere.

4.3.4.3   Monitor tropospheric reactive nitrogen levels

In a recent report (ftp://eospso.gsfc.nasa.gov/docs/chemistry.pdf) two key questions were identified relative to tropospheric reactive nitrogen.

1) Can we quantify the sources of reactive nitrogen in the upper troposphere, including . . . in situ aircraft emissions, in situ production by lightning, downward transport from the stratosphere, and upward transport of species emitted at the surface?

2) Can we improve our knowledge of the distributions of reactive nitrogen compounds in the troposphere through measurements and models . . . ?

Although improved terrestrial source estimates can aid in answering these questions, it is clear that more knowledge of the global distributions than can be obtained using aircraft in situ measurements alone will be required to reduce the uncertainties. Whereas sources of reactive N from biogenic sources (including fertilizers and other ecosystem or agronomic manipulations) can be modeled using EOS data, NO_x from lightning and aircraft cannot be so estimated (although lightning itself will be monitored). In particular, the lightning source is poorly constrained, and global observations of lightning and NO_x will be crucial for improving estimates of this source. In general, only if consistency can be achieved between 1) models of reactive N distributions using source estimates as input, 2) accurate and precise but episodic and regional in situ measurements, and 3) global climatological data from space, can closure of the reactive N budget be assumed. The EOS satellite contribution to this comes from the TES instrument, which can measure reactive N species in the limb-viewing mode. The limb mode will reduce the coverage and increase the minimum average altitude (because of clouds, which block the measurement and the larger footprint in the limb mode) relative to nadir viewing, but is required to achieve the requisite sensitivity.

4.3.5   Ozone: Its precursors and fate

4.3.5.1   Monitor ozone precursors

Ozone is different from the other species discussed earlier in the chapter as it is produced in situ in the atmosphere from precursor compounds, or, alternatively, transported from remote stratospheric sources into the troposphere. This makes understanding the sources, sinks, and distributions of ozone precursors in the atmosphere critical. One such precursor, reactive nitrogen, was discussed above and is particularly crucial. Over a wide range of chemical environments (leaving aside very low NO_x and very polluted air), as NO_x increases, O_3 will increase linearly. Thus the monitoring and development of a NO_x climatology, resolved by altitude, is a critical EOS product.

Other crucial species involved in O_3 formation include CO, CH_4, and the non-methane hydrocarbons (NMHCs), including biogenic isoprene and terpenes, and pollutant species. Of these, several can be monitored from space. CO has been measured successfully from space using a Shuttle instrument (Reichle et al. 1990; Fishman

et al. 1991). The MOPITT instrument on the EOS AM-1 platform will make measurements of CO at four levels in the atmosphere and will be supplemented by missions such as Mir using the MAPS instrument with less-than-global coverage. Figure 4.4 (pg. 180) shows a simplified scheme for tropospheric chemistry, indicating the key species or families of species involved in the tropospheric ozone cycle. The species are coded by whether they are observable or not. In addition, the species that require limb viewing (and so will be observed with lower spatial/temporal resolution, especially in the lower troposphere) are also noted.

Ozone itself must also be monitored. Ozone's horizontal distribution is quite variable, and satellite measurements show typical high ozone in industrially-polluted areas. A surprise finding from early tropospheric ozone measurements from space (using the tropospheric residual technique in which stratospheric ozone is subtracted from column ozone) was the presence of a tropical maximum, now believed to be the result of biomass burning (Andreae et al. 1988; Fishman et al. 1991). Because tropospheric ozone and especially lower-tropospheric ozone can be very variable in time and space, reflecting changing precursor sources and convective mixing upwards, space-based measurements are critical for understanding the climatology and temporal variability of ozone.

4.3.5.2   Monitor ozone vertical distribution

Ozone is distributed vertically in the atmosphere, with the majority (~90%) of atmospheric ozone located in the stratosphere. Because of mixing between the stratosphere and troposphere, the upper troposphere tends to have higher ozone levels than the lower, although this can be extremely heterogeneous because of the relatively short lifetime of ozone and its precursors, and because of the dynamic nature of stratosphere-troposphere exchange. Despite the generally increasing profile of ozone with height in the troposphere, local pollution can cause surface ozone levels as high as or higher than upper tropospheric levels. Ozone poses a different issue at different heights. High ozone in the boundary layer is a serious pollutant and is damaging to human health and ecosystems. Ozone in the mid-to-upper troposphere acts as a strong greenhouse gas, with a radiative forcing (if increases are evenly distributed in the troposphere) of 0.02 Wm^{-2} per ppbv change in O_3. Various estimates for the radiative forcing due to historical changes in O_3 are summarized in IPCC 1994 by Shine et al. (1995). Because of ozone's variable distribution in space, its positive radiative forcing effect can be quite localized.

Lower-stratospheric ozone depletion has the opposite effect. A loss of ozone in the lower stratosphere will lead to cooling, although the magnitude and (in extreme cases) the sign of the effect is dependent upon the shape of the ozone profile (Wang et al. 1993; Shine et al. 1995). Because of the sensitivity of the climate system to changes in the vertical distribution of ozone, and because of the biospheric significance of high boundary-layer ozone, vertical profiles of ozone are a key EOS product.

4.3.5.3   Monitor terrestrial emissions of O_3 precursors from soils, vegetation, and biomass burning

Changing terrestrial emissions from changing land use have the potential to alter tropospheric O_3 over much of the globe. As noted above, soil NO is potentially a significant factor, especially in the tropics, where deep convection may lift soil NO from the boundary layer to high altitudes, when otherwise most of it might be redeposited. As agriculture intensifies globally and nitrogen fertilizer use increases, this source could grow substantially. Terrestrial vegetation emits NMHCs, mainly isoprene and the terpenes, and, in the appropriate (high NO_x) chemical environment, these compounds react to form O_3. Biomass burning also releases a suite of compounds that can react to form ozone (hydrocarbons, methane, NO_x, CO, and the NMHCs), and contributes substantially to tropical ozone formation. In order to understand the contemporary atmosphere, and to monitor changes to sources that may impact atmospheric chemistry, spatial characteristics of terrestrial sources of ozone precursors are important data products. The approaches for NO_x were described above.

NMHC emissions are controlled by the biophysical environment, modified by the plant species considered. Different plant species emit different suites of NMHCs (Monson et al. 1995), with rates varying according to the physical environment of the leaf (Guenther et al. 1993) and the physiological state of the plant (Lerdau et al. 1995). The physical variables controlling leaf-level processes can be monitored as described above in Section 4.3.3, and models of NPP using satellite data form a strong foundation for assessing NMHC emissions. Species-specific emissions, as an input to model rates, require in situ determination, a process underway for many regions.

The basic biomass-burning measurement approaches are described above (4.3.2.1). Conversion of biomass burning detection to the quantification of trace-gas emissions requires the use of "emission factors"—the quantity of trace gas emitted per unit biomass burned or per unit CO_2 emitted. Considerable work has gone into the estimation of biome-specific emission factors for

Figure 4.4
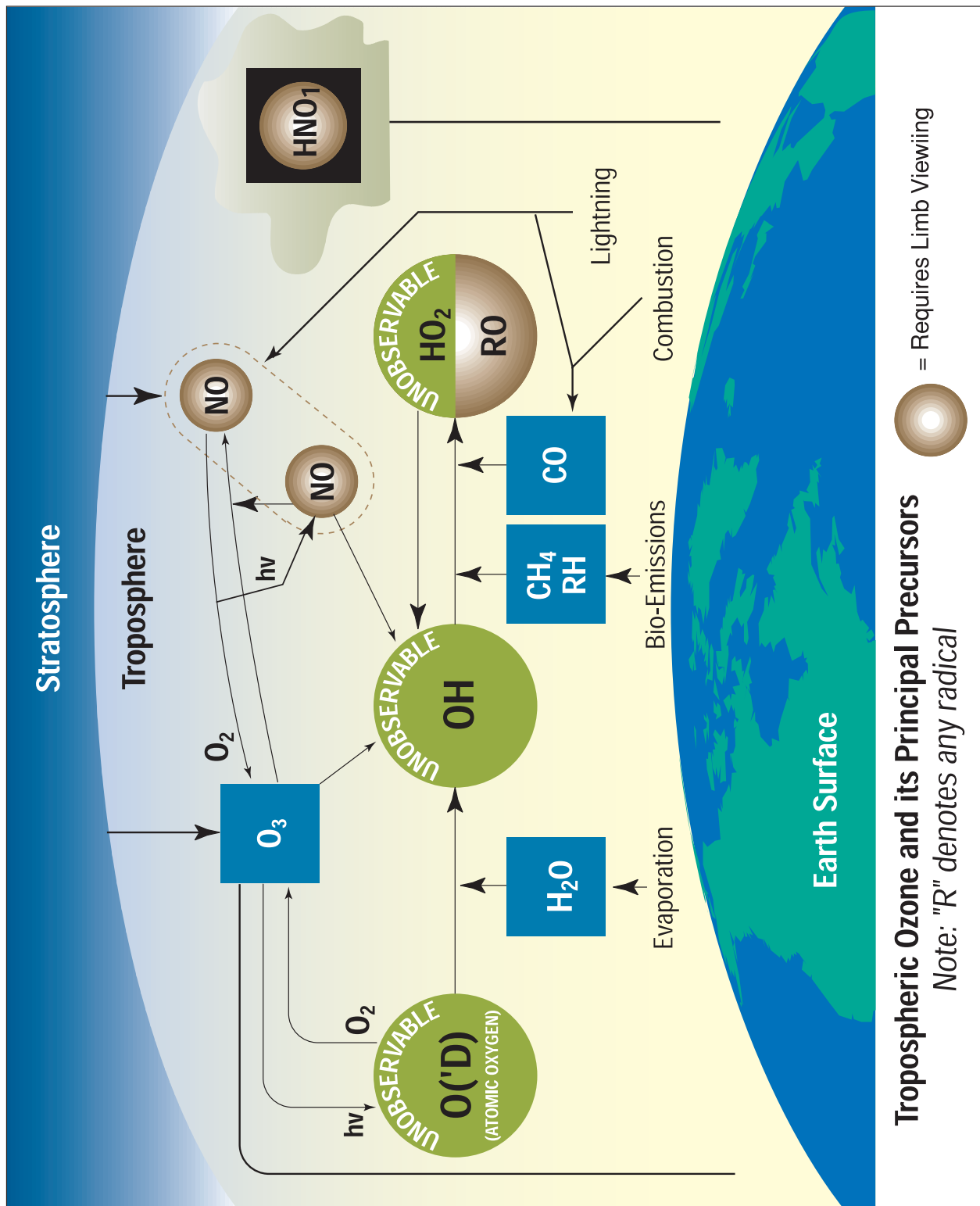
Tropospheric Ozone and its Principal Precursors
Note: "R" denotes any radical

A schematic of the tropospheric ozone cycle, indicating the key species or families of species involved. The species are coded by whether they are observable or not. The species that require limb viewing (and so will be observed with lower spatial/temporal resolution, especially in the lower troposphere) are also noted.

many chemical species in the Transport and Chemistry near the Equator over the Atlantic (TRACE-A) and South African Fire—Atmosphere Research Initiative (SAFARI) experiments in Southern Africa and South America; earlier work was done during Dynamique et Chimie de l'Atmosphere en Foret Equatoriale (DECAFE). These algorithms require information on extent of burning, temperature, and prior biomass levels. EOS data products, together with estimates of emission factors, will allow the production of fields of trace-gas release from biomass burning.

Finally, many O_3 precursors are derived from fossil-fuel combustion or other technological activity. While there is no current proposal to estimate such releases directly from remote sensing, remote observations of atmospheric chemistry (CO from MOPITT and the MAPS missions; O_3, and other compounds from TES) will aid in testing emission factors for surface and airborne sources.

4.4 EOS algorithms, observations, and required additional data

This section is intended to provide information on the anticipated EOS observations and data products supporting research on greenhouse gases and atmospheric chemistry. Many of the required algorithms and data products are documented in the land and hydrology and ocean chapters and we include here only cross-references. Other algorithms are still in development and are not planned for standard production as yet. For some of these only minimal information is now available (this includes especially the measurement of soil moisture and inundation where considerable uncertainty exists about the instrument capabilities and utility of products). Other data sets and algorithms are documented in this chapter.

4.4.1 The carbon cycle

4.4.1.1 Land measurements

4.4.1.1.1 Land cover and land-cover change
(See Chapter 5, "Land Ecosystems and Hydrology.")

4.4.1.1.2 Correlates of plant growth: FAPAR, LAI
(See Chapter 5, "Land Ecosystems and Hydrology.")

4.4.1.1.3 Biomass burning
(See 4.4.3.3.)

4.4.1.2 Ocean measurements

4.4.1.2.1 Ocean color
(See Chapter 3, "Oceanic Circulation, Productivity, and Exchange with the Atmosphere.")

4.4.1.2.2 Wind stress
(See Chapter 3, "Oceanic Circulation, Productivity, and Exchange with the Atmosphere.")

4.4.2 Methane and nitrous/nitric oxide

4.4.2.1 Surface correlates

4.4.2.1.1 Land cover and land-cover change
(See Chapter 5, "Land Ecosystems and Hydrology.")

4.4.2.1.2 Wetland productivity correlates: FIPAR and LAI
(See Chapter 5, "Land Ecosystems and Hydrology.")

4.4.2.2 Atmospheric retrieval of column methane
(See Section 4.4.3, below.)

4.4.3 Atmospheric chemistry and greenhouse gases

4.4.3.1 Methane and CO from MOPITT
This section describes the algorithm for retrieving vertical profiles of CO and the total column amount of CO and CH_4 from thermal emission and reflected solar radiation measurements by MOPITT in the 6.4-µm and 2.3-µm band of CH_4. Standard Level 2 products include 1) total column amounts of CO and CH_4 for the sunlit side of the orbit; and 2) vertical profiles of CO with a vertical resolution of about 3 km.

The MOPITT experiment has been described by Drummond (1992). The objective of MOPITT CO measurements is to obtain profiles with a resolution of 22 km horizontally, 3 km vertically, and with an accuracy of 10%

throughout the troposphere. A CO total-column-amount measurement will also be made with a 10% accuracy. For CH_4, the objective is to measure the column in the troposphere to a precision of better than 1%, with a spatial resolution similar to that of the CO measurement. The column amounts of CO and CH_4 will only be available on the sunlit side of the orbit as standard Level 2 MOPITT products.

The concentration of CO in the Earth's atmosphere has been changing mainly because of increased human activities (Khalil and Rasmussen 1994). The full range of the effects of the increased concentration of CO is not fully understood at the present time, but it is believed that CO is photochemically active and plays a major part in the concentration of OH radicals in the troposphere. Increased CO may deplete tropospheric OH radicals, thereby reducing the yearly removal of many natural and anthropogenic trace species. In particular, this effect may add to the increase of CH_4, which in turn could further reduce OH concentration. Increased CO may also indirectly intensify global warming and perturb the stratospheric ozone layer by increasing the lifetime of trace gases such as CH_4, CH_3Cl, CH_3CCl_3, and the HCFCs and HFCs. Global measurements of CO and CH_4 will undoubtedly shed light on the concentration of OH, which is one of the most important and difficult species to measure from space due to its very low concentration. Those measurements will enhance our knowledge of the chemistry of the troposphere and particularly how it interacts with the surface/ocean/biomass systems, atmospheric transports, and the carbon cycle. Global CO and CH_4 measurements from MOPITT will also be used in parallel modeling efforts to advance our understanding of global tropospheric chemistry and its relationship to sources, sinks, and atmospheric transports, which can be determined from other data. Understanding their biogeochemical cycles and their intimate interrelation with each other and with climate will lead to better predictions of possible effects of anthropogenic activities.

The possibility of remotely measuring CO profiles in the troposphere from spaceborne platform observations of thermal-infrared emission/absorption was first suggested by Ludwig et al. in 1974. Success of MAPS on the second Space Transport System engineering test flight (STS-2) of the Shuttle in November 1981 proved the feasibility of inferring the CO profile from measurements by a nadir-viewing instrument (Reichle et al. 1986). The instrument employed is a gas filter radiometer operating in the 4.7-μm region of the CO fundamental band with a passband from 2080 to 2220 cm^{-1}. At the surface, the instantaneous field of view is approximately 20-by-20 km. Successive MAPS experiments provided more global tropospheric CO measurements and further demonstrated the importance and feasibility of CO measurements from space.

Even though MAPS experiments have provided important global CO measurements for global tropospheric chemistry study, limited coverage, with only the average CO mixing ratio in the middle of the troposphere, is not adequate, and multiple-level CO measurements that would resolve the troposphere into several layers are needed. MOPITT is an instrument designed to meet this requirement and provide global CO measurements of the lower, middle, and upper troposphere and daytime total columns of CO and CH_4. The MOPITT retrieval algorithm is based on proven retrieval techniques, such as the maximum likelihood method (Rodgers 1976), and is designed to maximize scientific return of the MOPITT experiment with state-of-the-art retrieval techniques.

4.4.3.1.1 Instrument characteristics

MOPITT, on the AM-1 platform, measures upwelling thermal emission from the atmosphere and surface in the longwave channels, and reflected solar radiation in the shortwave channels (radiation that has passed through the atmosphere, been reflected at the surface, and been transmitted back up through the atmosphere). Total atmospheric transmittance derived from reflected sunlight measurements is a convenient way to determine the total column amount of a trace gas. This technique requires that the target gas have a spectral band in a region with large solar radiance, and that the total optical depth along such a path not be too large. Methane has an overtone band near 2.2 μm with a measurable but not-too-large total absorption for such a path. Similarly, CO has its first overtone band at 2.3 μm, which is also suitable. For vertical profiling, the requirement is that significant and measurable portions of the signal must originate in different atmospheric layers, which means that there must also be a source of radiation in the atmosphere. Thermal emission is a radiation source, and the CO fundamental band at 4.7 μm has enough opacity to determine atmospheric amounts, as demonstrated by Reichle et al. (1986, 1990).

All three bands are in regions of the spectrum with other bands, and the lines of the gases of interest are mixed with those of interfering species. It would be possible, in principle, to measure the total emission or transmission of the species of interest, and correct for the contributions of interfering species. However, the contributions of other species are often larger than those of the gases of interest, and their amounts are often not known with sufficient accuracy. The uncertainties of the corrections may significantly degrade, or even mask, changes due to the gas of interest.

MOPITT is designed to meet this challenge by enhancing the sensitivity of the instrument to the gas of interest. Since all gases in the atmosphere are emitting/absorbing simultaneously, it is essential that the effect of the gas of interest can be separated out from the general radiation field. Further, the information about the vertical distribution of the gas is contained within the shape, which generally requires high spectral resolution. High spectral resolution leads to low signal-to-noise, which means low instrument sensitivity. Therefore, high-sensitivity and high-spectral-resolution requirements for tropospheric trace species remote sensing are difficult to implement with conventional dispersing instruments.

Correlation radiometry (CR), a non-dispersive spectroscopic technique, offers the promise of high effective spectral resolution with a high signal-to-noise ratio achieved by higher throughput through analog addition of signals from many spectral lines. In CR, a cell containing a sample of the target gas is placed in the optical train ahead of the detector. The gas in the cell absorbs the incoming radiation at the frequencies of its spectral lines. By varying the amount of gas in the cell between a higher and lower amount, a difference signal can be obtained due to the difference in absorption by the target gas lines. The difference signal is identical to the output of a system in which the gas cell and its modulator are replaced by an optical filter which only responds at the frequencies of the target gas lines. A further feature is that if the cell gas pressure is low, the difference is primarily near the center of the line, while for higher cell pressure the difference is in the line wings. This can be used to obtain information on the vertical distribution of the target gas.

MOPITT makes use of two methods to modulate the gas amounts in the cell, depending on cell pressure. For low pressures (< 100 hPa) the pressure is modulated through the use of pressure-modulated cells, described in detail by Taylor (1983). For high pressures, the cells are modulated by changing the length of the gas cell (Drummond, 1989).

4.4.3.2 Ozone and ozone precursors from TES

Figure 4.4 shows the principal pathways through which tropospheric ozone is created, transported, and destroyed. As the figure shows, the chemistry is very complex, and, unfortunately, several key species (notably atomic oxygen in the $O(^1D)$ state and the OH and HO_2 radicals) are unobservable by any current remote sensor; thus, their concentrations must be inferred through a combination of models and observed concentrations of precursor species. Furthermore, the equally important active nitrogen species NO, NO_2, and HNO_3, and most of the oxygenated hydrocarbons ("RO") can only be observed by limb viewing because of their very low concentrations (typically parts-per-trillion). On the other hand, species such as O_3 itself, H_2O, CO, and the more-abundant simple hydrocarbons can be observed both in the nadir and at the limb. This is important because limb viewing rarely penetrates below about 5 km (because of cloud interference), but many of the critical interactions take place closer to the surface. Thus, while both capabilities are needed to provide inputs to the models, it is essential that the air masses observed in both limb and nadir modes be, as nearly as possible, the same because much of the chemistry is quite localized. TES has been specifically designed to provide this capability.

4.4.3.2.1 TES

TES is an infrared (650 - 3050 cm^{-1}; 3.3 - 15.4 μm), high-resolution (0.025 cm^{-1}), imaging (1 × 16 pixels) Connes'-type Fourier Transform Spectrometer intended for the near-simultaneous measurement and profiling of the global three-dimensional concentrations of those molecules key to the production and destruction of tropospheric ozone, with especial emphasis on the reactive nitrogen species (Table 4.1, pg. 190). On regional and local scales, TES may (as a goal) measure additional species that are sporadic or otherwise not well-quantified (Table 4.2, pg. 190). Even more species will certainly be measurable but they are generally of minor interest. Nevertheless, they must be accounted for in the retrieval process because they contribute to the received radiance, and their neglect can compromise the accuracy of the retrieved concentrations of the major species.

TES operates by natural thermal emission (650 - 2450 cm^{-1}; 4.1 - 15.4 μm) and by solar reflection (2000 - 3050 cm^{-1}; 3.3 - 5.0 μm) when appropriate. TES will obtain its data in single scans of four seconds each in downlooking (nadir ± 45°) operations and in 16 seconds while staring at the trailing limb (0 - 33 km). Longer integrations (up to 221 seconds) by scan-averaging are possible for improved sensitivity, or multiple scans over the same interval can be used to investigate time variability. Spatial variability can be studied by "stacking" footprints contiguously to generate North-South transects up to 2700 km long. Spatial resolution from the EOS 705-km orbit is interchangeably 0.5 km cross-track × 5 km in-track or 2.5 × 25 km in the nadir (per each of 16 contiguous pixels) and 2.3 km high × 23 km (parallel to the Earth's surface) at the limb, providing 16 simultaneous measurement levels from the surface to about 33 km.

4.4.3.2.2 The extraction of concentration profiles from infrared spectra

Most modern retrieval algorithms for the extraction of concentration profiles operate on similar principles: a "first guess" physical and chemical compositional profile of the atmosphere is set up (the source may be climatology, a previously retrieved set, or, sometimes, sonde profiles), and, incorporating known instrumental properties such as spectral resolution and instrumental line shape, a model spectrum is generated through a forward solution of an appropriate version of the equation of radiative transfer. The model calculation is compared to the actual data and the model is iterated until the two match to within some prescribed limit. The differences among algorithms generally lie in: a) the exact character of the inevitable approximations inherent in any numerical calculation, and b) the methods used to indicate that convergence has occurred. It should further be noted that the problem is ill-conditioned—it can never be demonstrated that the solution is unique (one can "drop" into local minima of the solution space). Thus verification and correlative measurements are a crucial part of the operation.

Measurements in the troposphere can, however, take advantage of the fact that spectral lines formed below about 20 km exhibit significant pressure-broadening (see Figure 4.5). Thus, species whose stratospheric abundance greatly exceeds that in the troposphere (such as O_3 itself) can nevertheless be discriminated provided that the spectral resolution suffices to make this possible.

The shape of pressure-broadened lines is reasonably well described by the Lorentz Function:

$$1) \quad k_L(n - n_0) = \frac{S(n_0)\Sigma a_L}{p\Sigma[(n - n_0)^2 + a_L{}^2]}$$

where k_L is the absorption coefficient, S is the line strength (tabulated), n is frequency (normally in cm^{-1}), n_0 is the frequency of the line center, and a_L is the broadening coefficient (defined as the half-width at half-maximum of the function).

a_L, which is directly proportional to pressure, is determined empirically through laboratory investigations and is tabulated at STP because it also has a weak (and often unknown) temperature dependence (roughly as $T^{1/2}$). The absorption A (= 1 - transmission) of the gas is related to the absorption coefficient by:

$$2) \quad A(n - n_0) = 1 - \exp[-k(n - n_0).L]$$

where L is the number of molecules of the particular species in the line of sight (at constant temperature and pressure).

Now, it is a curious (but quantum-mechanically explicable) property of a_L that its value is nearly independent of species and frequency (wavelength) and takes a value of about 0.05 cm^{-1} near the Earth's surface. Thus, when the product of k_L and L is small (a so-called "weak line"), the full width at half maximum depth of the spectral line is $2a_L$ (0.1 cm^{-1}) for all molecules anywhere in the spectrum.

There is only one class of spectrometer that meets the requirements of broad spectral coverage and frequency-independent spectral resolution—a Fourier Transform Spectrometer (FTS). Thus, TES has been designed to be an FTS.

As examples of how the retrieval process operates, Figures 4.6 through 4.11 (pp. 186-187) show simulated limb retrievals of many of the species important to tropospheric chemistry (the error bars are based on expected TES performance but do not include any sources of systematic error). Again, it must be emphasized that those profiles that are shown as going to the surface will rarely, in practice, do so because of cloud interference.

4.4.3.3 Biomass-burning sources of gases (including CO_2)

The MODIS fire product uses the special fire channel at 3.9 μm that saturates at 500 K and the high gain of the 11-μm channel. During the night the fire product will use also the 1.65- and 2.15-μm channels. The analysis is based on a 10×10-pixel box comparing the fire-apparent temperatures in these spectral bands to the background temperatures and their standard deviation. The product includes daily fire occurrence (day/night), the logical criteria used for the fire selection (day/night), and fire location. For fires that are high enough above the detection limit, the fire spectral apparent temperatures will be converted into the total emitted energy from the fire and the smoldering/flaming ratio. The fires are classified into fire classes based on their strength; for each class the ratio between smoldering and flaming stage is computed from empirical field information. This information is expected to be helpful in estimation of the spatial and temporal distribution of fires in different ecosystems and for the estimation of the emissions of trace gases and particulates from the fires.

The product also includes: composite ten-day-and-night fire occurrence (full resolution); composite monthly day-and-night fire occurrence (full resolution); gridded 10-km summary per fire class (as described above; daily/ten day/monthly) count of the number of fires in each class and the ratio between smoldering and flaming for the combination of all the fires in the class; and gridded 0.5-degree summary of fire counts per class (daily/ten-day/monthly), and smoldering/flaming per class.

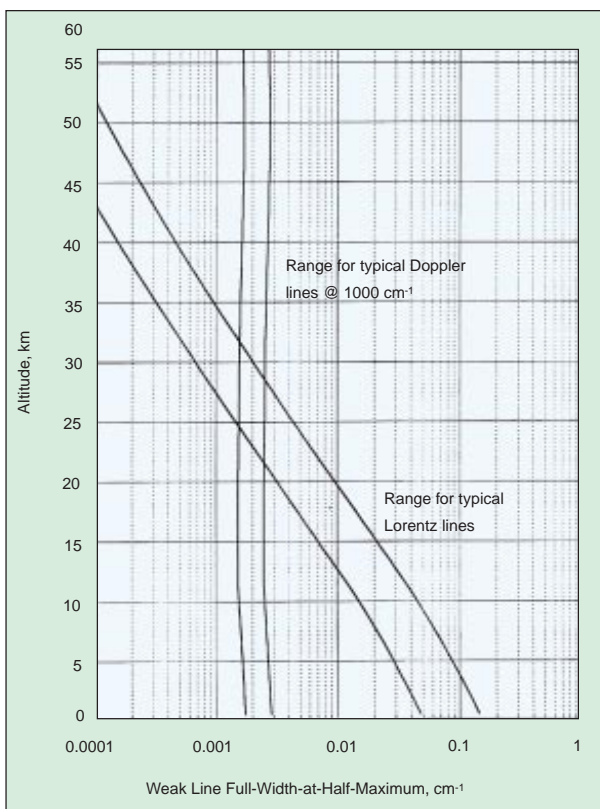# 4.5 Synthesis and integrative modeling: status and needs

4.5.1 Introduction

The unique aspect of the topics discussed in this chapter is the degree of interdisciplinary integration across the EOS program they require. Even a first-order analysis of the carbon cycle requires addressing fundamental problems of ocean physics and biology, terrestrial ecology and biophysics, and atmospheric transport and measurements. Because the carbon cycle is driven by industrial processes, transportation, energy use, land-use change, and other anthropogenic processes, the human dimensions of the problem are also central. Understanding the changing ozone content of the troposphere is likewise integrative and interdisciplinary. Like the carbon cycle, changing atmospheric chemistry is driven by changing land use and "industrial ecology.' Other sources and many of the sinks for trace gases are biological and require fundamental ecological knowledge in order to understand rates and extrapolate them correctly in time and space (Andreae and Schimel 1989). The effects of ozone on climate and the biosphere are determined by the horizontal and vertical distribution of O_3, which is controlled by 1) the geography of sources, 2) chemical reactions in the atmosphere, 3) transport and mixing by physical processes, and 4) physical, biological, chemical, and dynamic (e.g., mixing into the stratosphere, loss at the surface) sinks.

Many of the most critical processes for biogeochemistry in all three domains—oceans, land, and atmosphere—are extremely heterogeneous in time and space, thus requiring global time-series monitoring. These processes are largely invisible to direct remote observation. Such key "invisible" processes include, but are not limited to 1) respiration from dead organic matter on land, 2) mixing of carbon from the surface to deeper ocean layers, and 3) the atmospheric concentrations of the hydroxyl radical. Because of this invisibility, a central tool in the overall strategy is to use available data from remote and in situ sensors to constrain models, and to use models to interpolate in time and space as a means to estimate these invisible processes. This procedure must be continually evaluated against independent observations, made in situ when needed, which, in addition to testing the ability of models to interpolate and estimate additional variables, also allow the diagnosis of errors and biases. This, in turn, provides information that can improve and reduce the uncertainties when models are used in a predictive or extrapolation mode.

4.5.2 An EOS strategy for integrative models of biogeochemistry

The problems inherent in the carbon cycle and other greenhouse gases require integration not only within the "interdisciplinary" investigations that are a main component of the EOS program, but across multiple IDS teams and with instrument team science and algorithm investigations as well. These problems also require integration of non-EOS in situ data. The components required for CO_2, methane, N_2O, NO, NMHC, and O_3 modeling and analysis, however, have much in common. Below, we outline two major thrusts to integrate EOS data and large-scale modeling for the carbon and ozone cycles. These do not exhaust the important integrative research and application areas, but exemplify how EOS data, process understanding, and global models can be used synergistically.
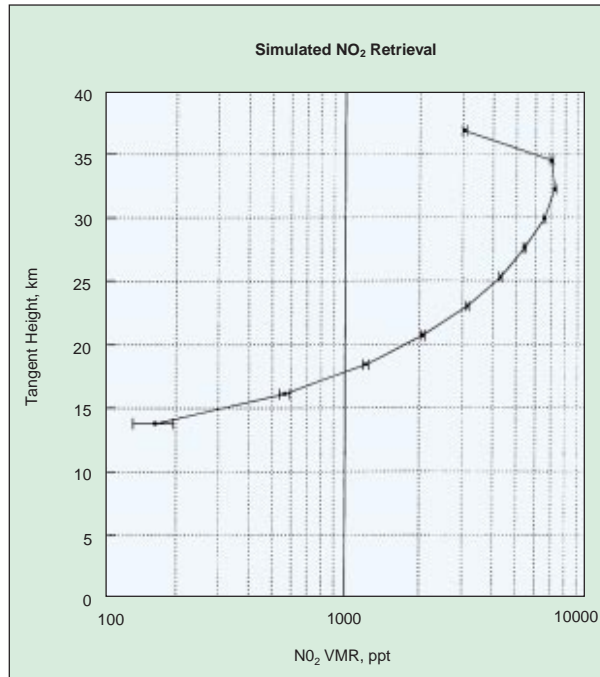
4.5.2.1 The carbon cycle

Figure 4.12 (pg. 188) shows how EOS data and models can be integrated. Information on the physical atmosphere provides either direct or assimilated information on the

Variation of spectral line widths as a function of altitude *(TES Science Team).*
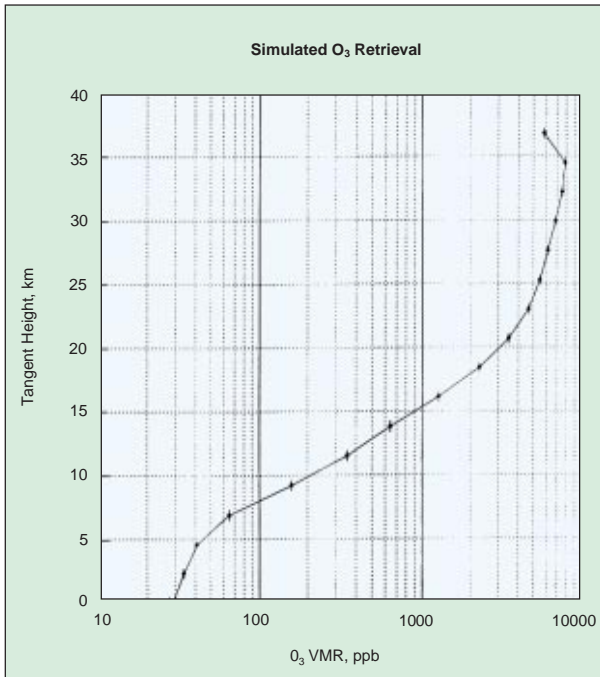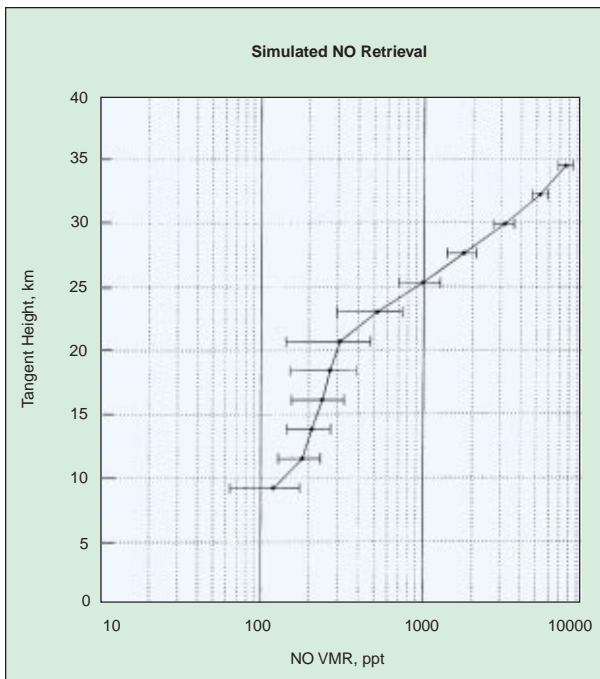
FIGURE 4.6

Simulated limb retrieval of ozone. (The error bars are based on ex-
pected TES performance but do not include any sources of systematic
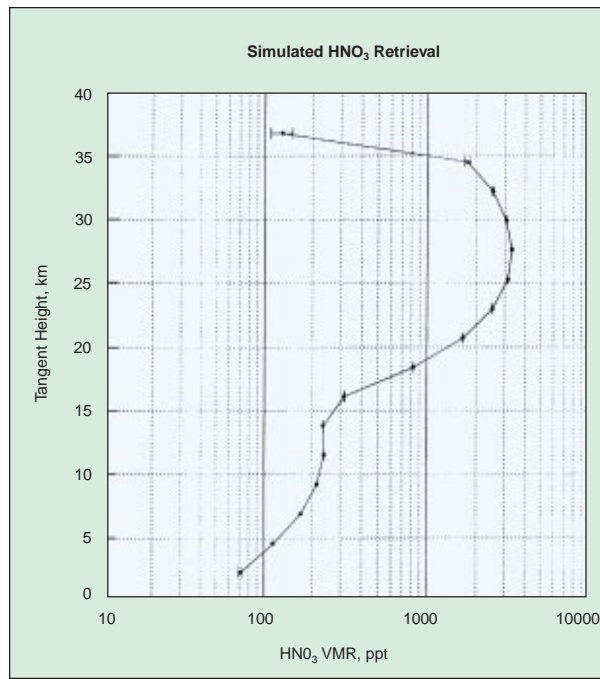error.) *(TES Science Team.)*

FIGURE 4.7

Simulated limb retrieval of NO. Error bars as in Figure 4.6.
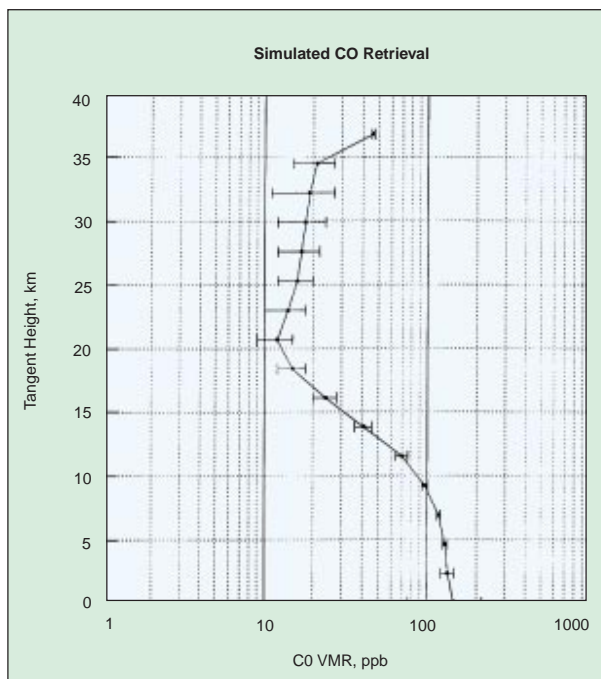*(TES Science Team.)*

FIGURE 4.8

Simulated limb retrieval of NO_2. Error bars as in Figure 4.6.
(TES Science Team.)

FIGURE 4.9

Simulated limb retrieval of HNO_3. Error bars as in Figure 4.6.
(TES Science Team.)

FIGURE 4.10

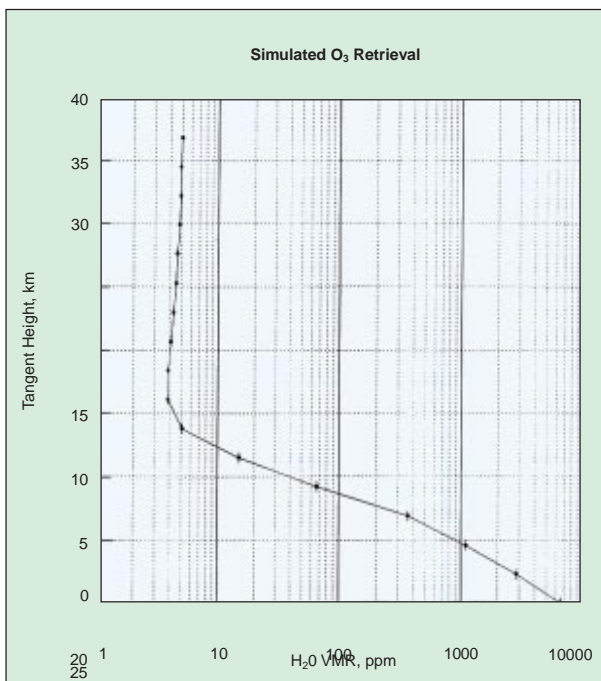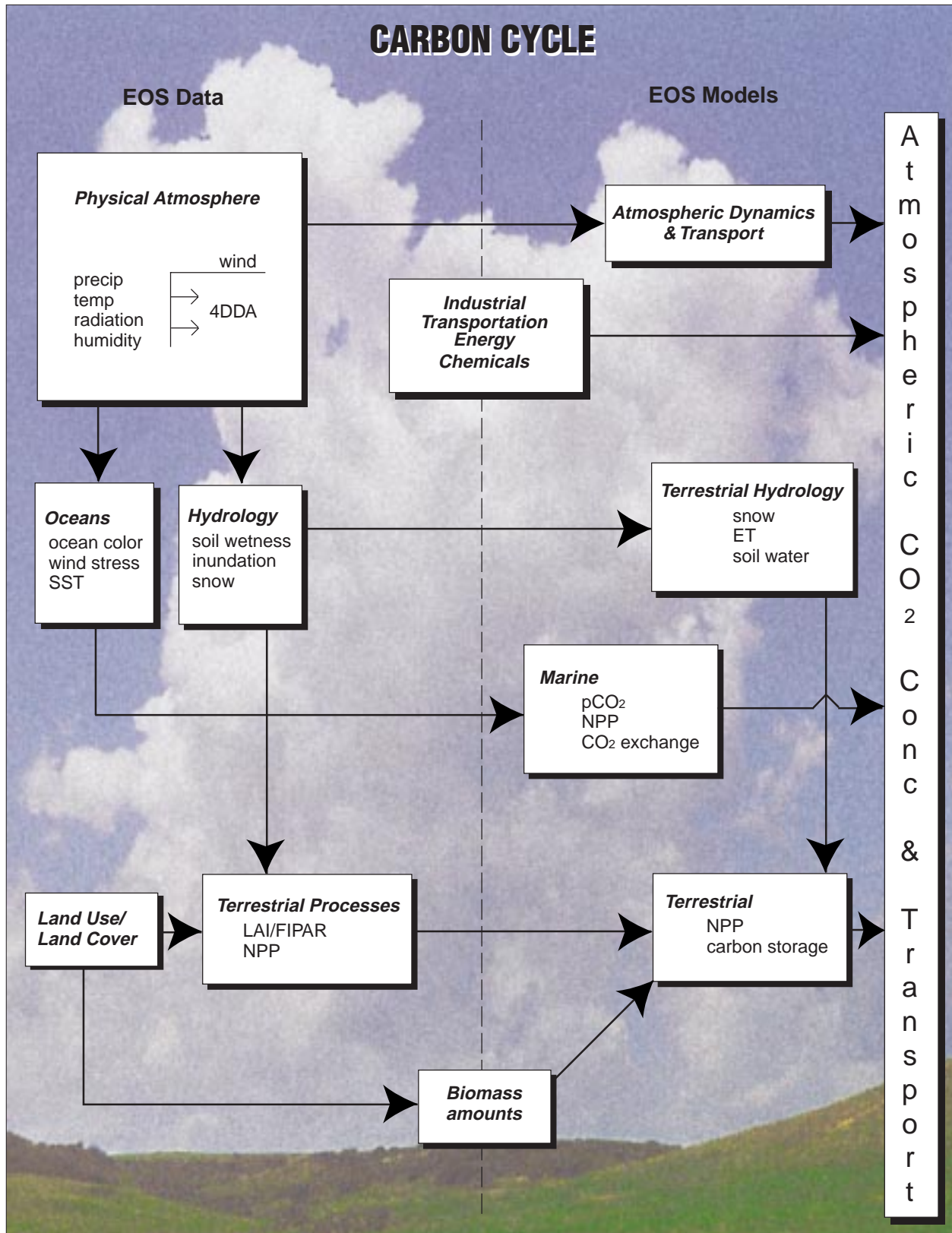Simulated limb retrieval of CO. Error bars as in Figure 4.6. *(TES Science Team.)*

FIGURE 4.11

Simulated limb retrieval of H_2O. Error bars as in Figure 4.6. *(TES Science Team.)*

critical land-surface-climate variables, including temperature, radiation, and precipitation, wind stress, and other factors influencing the terrestrial biophysical and marine gas-exchange environment. For the terrestrial system, these variables, plus snow, surface wetness, and other retrievals, may be further analyzed to produce fields of hydrological variables such as inundation and soil moisture. Remote observations of land cover and land-cover change are combined with either in situ or remote (radar) estimates of biomass to produce a carbon flux from land-use change. Climate information is combined with land-cover data as inputs into ecosystem models to compute terrestrial carbon storage changes. Together, the ocean, ecosystem, and land-use change fluxes are combined to produce spatial maps of terrestrial sources and sinks of CO_2, with fossil-fuel and cement sources also included from statistical data. The distributions of CO_2 in the atmosphere (measured in situ) may then be further analyzed using transport observations from the physical atmosphere for consistency with the modeled sources and sinks. This approach will link the existing land, atmosphere, and ocean activities.
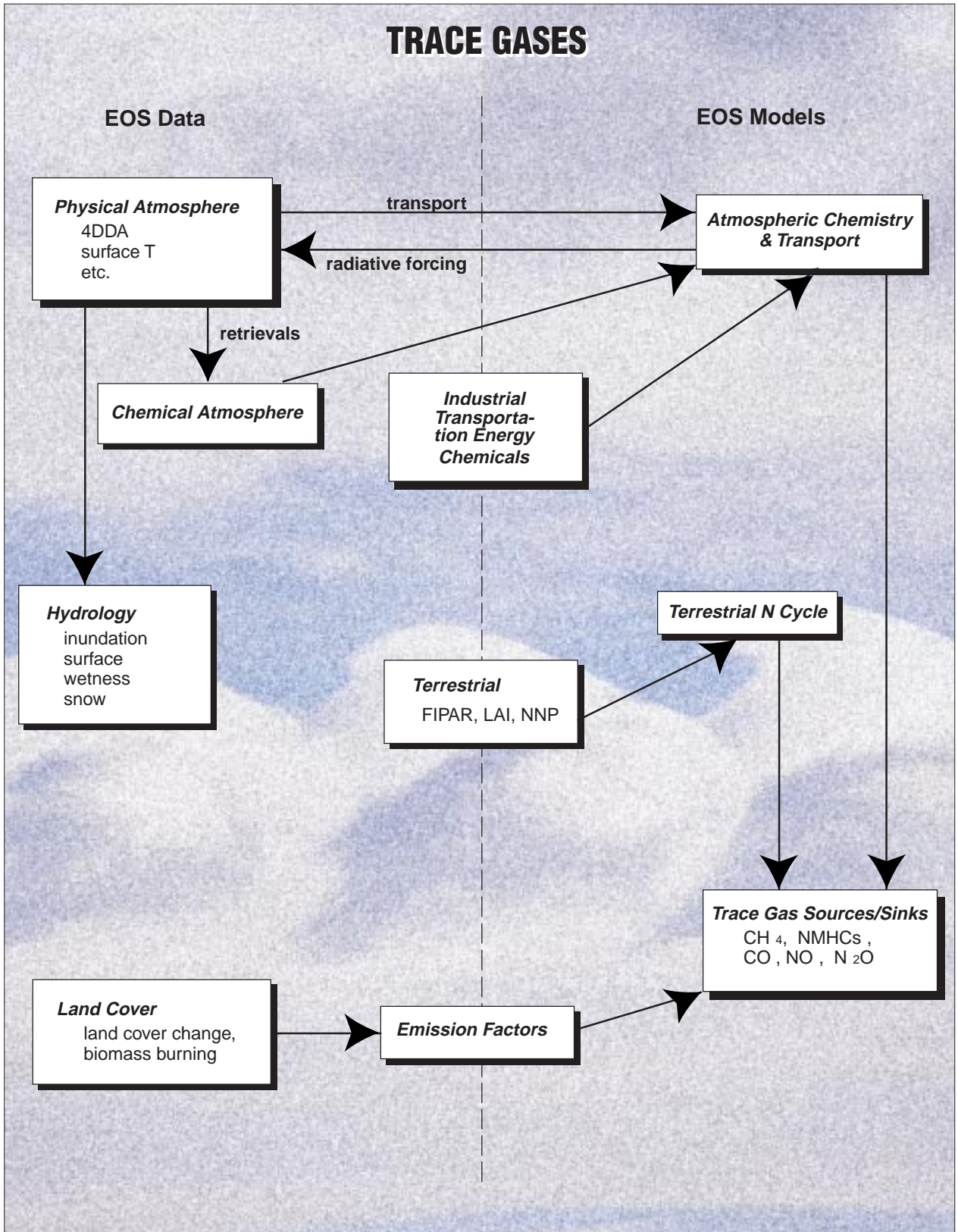
4.5.2.2   Trace gases

Figure 4.13 (pg. 189) shows a similar scheme for trace gases and the ozone cycle. Information about the physical atmosphere is used to compute biophysical conditions for the land surface and aquatic systems that govern trace-gas emissions, as for the carbon cycle. This information, together with information retrieved about vegetation and ecosystems, is used as input into models of the terrestrial nitrogen cycle and plant physiology. These in turn can be used to compute the fluxes of nitrogen- and carbon-based trace gases, both greenhouse gases and gases involved in the ozone cycle. These fluxes can be used as inputs to atmospheric chemical transport models, possibly coupled to climate models. Direct retrievals of the distributions of greenhouse gases from TES, MOPITT, High-Resolution Dynamics Limb Sounder (HIRDLS), and other instruments can also be passed to the chemical transport models. Finally, anthropogenic gases from industrial, transportation, energy, chemical, and other sectors are also passed to the chemical transport models. This system can address a number of questions, including: 1) Can we explain current distributions of ozone and other key tropospheric gases from known sources and sinks of ozone and precursors? 2) How might changing land use affect future tropospheric chemistry? and 3) How are changing sources, including aircraft, affecting the vertical distribution of ozone?

Figure 4.12

CARBON CYCLE

Integration of EOS data and models for the carbon cycle.

FIGURE 4.13

TRACE GASES

EOS Data

EOS Models

Physical Atmosphere
4DDA
surface T
etc.

transport

Atmospheric Chemistry & Transport

radiative forcing

retrievals

Chemical Atmosphere

Industrial Transporta-tion Energy Chemicals

Hydrology
inundation
surface
wetness
snow

Terrestrial N Cycle

Terrestrial
FIPAR, LAI, NNP

Trace Gas Sources/Sinks
CH_4, NMHCs,
CO, NO, N_2O

Land Cover
land cover change,
biomass burning

Emission Factors

Integration of EOS data and models for trace gases.

Table 4.1: TES Standard Data Products

O_x	H_xO_y	C-compounds	N-compounds
O_3 (3 ppb)	H_2O (0.5-50 ppm)	CO (3 ppb)	NO
		CH_4 (14 ppb)	NO_2
			HNO_3

Numbers in parentheses are estimated Volume Mixing Ratio (VMR) sensitivities based on a combination of limb and nadir observations; accuracies are expected to be in the 5 - 20% range. Altitude coverage is 0 - 33 km except for NO_y.

Table 4.2: TES Special Data Products

H_xO_y	C-compounds	N-compounds	Halogen-compounds	S-compounds
H_2O_2	CO_2	HNO_4	HCl*	SO_2
HDO	C_2H_6	NH_3	HF*	COS
	C_2H_2	HCN	H_2S*	
	HCOH	N_2O**		
	HCOOH			
	CH_3OH			
	PAN			

Sensitivities are TBD; accuracies are expected to be no better than 10% — * Volcanic plume column densities only — ** Control (VMR known)

References

Andreae, M. O., and D. S. Schimel, 1989: Exchange of trace gases between terrestrial ecosystems and the atmosphere, *Dahlem Workshop Reports - Life Sciences Research Reports*, **47**, 347.

Andreae, M. O., E. V. Browell, G. L. Garstang, R. C. Gregory, R. C. Harriss, G. F. Hill, D. J. Jacob, M. C. Pereira, G. W. Sachse, A. W. Setzer, P. L. Silva Dias, R. W. Talbot, A. L. Torres, and S. C. Wofsy, 1988: Biomass-burning emissions and associated haze layers over Amazonia, *J. Geophys. Res.*, **93**, 1509-1527.

Anonymous, 1996: *World Climate News*, **9**.

Aselmann, I., and P. J. Crutzen, 1989: Global distribution of natural freshwater wetlands and rice paddies, their net primary productivity, seasonality, and possible methane emissions, *J. Atmos. Chem.*, **8**, 307-358.

Asrar, G., and R. Greenstone, 1995: *MTPE/EOS Reference Handbook*, NASA, MTPE, EOS, Greenbelt, MD.

Bartlett, K. B., and R. C. Harriss, 1993: Review and assessment of methane emissions from wetlands, *Chemosphere*, **26**, 261-320.

Braswell, B. H., 1996: Global terrestrial biogeochemistry: perturbations, interactions, and time scales, Ph.D. Thesis, University of New Hampshire, Department of Earth Sciences, Durham, NH.

Choudhury, B. J., 1989: Monitoring global land surface using Nimbus-7 37 GHz data, theory and examples, *Int. J. of Remote Sensing*, **10**, 1579-1605.

Ciais, P., P. P. Tans, M. Trolier, J. W. C. White, and R. J. Francey, 1995: A large Northern Hemisphere terrestrial CO_2 sink indicated by $^{13}C/^{12}C$ of atmospheric CO_2, *Science*, **269**, 1098-1102.

Conway, T. J., P. Tans, L. S. Waterman, K. W. Thoning, D. R. Buanerkitzis, K. A. Maserie, and N. Zhang, 1994: Evidence for interannual variability of the carbon cycle from the NOAA/CMDL global air sampling network, *J. Geophys. Res.*, **99D**, 22831-22855.

Dacey, J. W. H., and M. J. Klug, 1979: Methane efflux from lake sediments through water lilies, *Science*, **203**, 1253 - 1255.

Davidson, E. A., 1992: Sources of nitric oxide and nitrous oxide following wetting of dry soil, *Soil Science Society of America Journal*, **56**, 95-102.

Denning, A. S., I. Y. Fung, and D. Randall, 1995: Latitudinal gradient of atmospheric CO_2 due to seasonal exchange with land biota, *Nature*, **376**, 240-243.

Dlugokencky, E. J., L. P. Steele, P. M. Lang, and K. A. Masarie, 1994: The growth rate and distribution of atmospheric methane, *J. Geophys. Res.*, **99**, 17021-17043.

Drummond, J. R., 1989: Novel correlation radiometer: the length-modulated radiometer, *Applied Optics*, **28**, 2451-2452.

Drummond, J. R., 1992: Measurements of pollution in the troposphere (MOPITT), *The Use of EOS for Studies of Atmospheric Physics*, (J. C. Gille and G. Visconti, Eds.), North Holland, Amsterdam, pp. 77-101.

Eswaran, H., E. Van den Berg, and P. Reich, 1993: Organic carbon in soils of the world, *Soil Science Society of America Journal*, **57**, 192-194.

Firestone, M. K., and E. A. Davidson, 1989: Microbiological basis of NO and N_2O production and consumption in soil, *Exchange of Trace Gases between Terrestrial Ecosystems and the Atmosphere*, (M. O. Andreae and D. S. Schimel, Eds.), John Wiley & Sons, New York, pp. 7-22.

Fisher, M. J., I. M. Rao, M. A. Ayarza, C. E. Lascano, J. I. Sanz, R. J. Thomas, and R. R. Vera, 1994: Carbon storage by introduced deep-rooted grasses in the South American savannas, *Nature*, **371**, 236-238.

Fishman, J., K. Fakhruzzaman, B. Cros, and D. Nganga, 1991: Identification of widespread pollution in the Southern Hemisphere deduced from satellite analysis, *Science*, **252**, 1693-1696.

Glantz, M. H., R. W. Katz, and N. Nicholls, (Eds.), 1991: *Teleconnections Linking Worldwide Climate Anomalies: Scientific Basis and Societal Impact*, Cambridge University Press, New York.

Guenther, A. B., P. R. Zimmerman, P. C. Harley, R. K. Monson, and R. Fall, 1993: Isoprene and monoterpene emission rate variability: model evaluations and sensitivity analyses, *J. Geophys. Res.*, **98**, 12609-12617.

Hamilton, S. K., S. J. Sippel, and J. M. Melack, 1996: Inundation patterns in the Pantanal wetland of South America determined from passive microwave remote sensing, *Archives of Hydrobiology*, **137**, 1-23.

Hess, L. L., J. M. Melack, and D. S. Simonett, 1990: Radar detection of flooding beneath the forest canopy: a review, *Int. J. of Remote Sensing*, **5**, 1313-1325.

Hess, L. L., J. M. Melack, S. Filoso, and Y. Wang, 1995: Delineation of inundated area and vegetation along the Amazon floodplain with the SIR-C synthetic aperture radar, *IEEE Trans Geosci. Remote Sens.*, **33**, 896-904.

Houghton, R. A., 1995: Effects of land-use change, surface temperature, and CO_2 concentration on terrestrial stores of carbon, *Biotic Feedbacks in the Global Climatic System: Will the Warming Feed the Warming?*, (G. M. Woodwell and F. T. Mackenzie, Eds.), Oxford University Press, New York, pp. 333-350.

INPE, 1992: Deforestation in Brazilian Amazonia, Instituto Nacional de Pesquisas Espaciais, São Paulo, Brazil.

Jackson, T. J., and T. J. Schmugge, 1991: Vegetation effects on the microwave emission of soils, *Remote Sens. Environ.*, **36**, 203-212.

Jackson, T. J., 1993: III. Measuring surface soil moisture using passive microwave remote sensing, *Hydrological processes*, **7**, 139-152.

Jones, P. D., T. M. L. Wigley, and K. R. Briffa, 1994: Global and hemispheric temperature anomalies — land and marine instrumental records, *Trends '93: A Compendium of Data on Global Change*, (T. A. Boden, D. P. Kaiser, R. J. Sepanski, and F. W. Stoss, Eds.), ORNL/CDIAC-65. Carbon Dioxide Information Analysis Center, Oak Ridge National Laboratory, Oak Ridge, Tenn., pp. 603-609.

Keeling, C. D., J. F. S. Chin, and T. P. Whorf, 1996: Increased activity of northern vegetation inferred from atmospheric CO_2 measurements, Nature, **382**, 146-149.

Keeling, C. D., T. P. Whorf, M. Wahlen, and J. van der Plicht, J., 1995: Interannual extremes in the rate of rise of atmospheric carbon dioxide since 1980, *Nature*, **375**, 666-670.

Keller, M., E. Veldkamp, A. M. Weltz, and W. A. Reiners, 1993: Effect of pasture age on soil trace-gas emissions from a deforested area of Costa Rica, *Nature*, **365**, 244-246.

Khalil, M. A. K., and R. A. Rasmussen, 1994: Global decrease of atmospheric carbon monoxide, *Nature*, **370**, 639-641.

Lerdau, M., P. Matson, R. Fall, and R. Monson, 1995: Ecological controls over monoterpene emissions from douglas-fir (*Pseudotsuga menziesii*), *Ecology*, **76**, 2640-2647.

Ludwig, C. B., M. Griggs, W. Malkmus, and E. R. Bartle, 1974: Measurement of air pollutants from satellites, 1. Feasibility considerations, *Applied Optics*, **13**, 1494.

Luizão, F., P. Matson, G. Livingston, R. Luizão, and P. Vitousek, 1989: Nitrous oxide flux following tropical land clearing, *Global Biogeochemical Cycles*, **3**, 281-285.

McBride, J. L., and N. Nicholls, 1983: Seasonal relationships between Australian rainfall and the southern oscillation, *Mon. Wea. Rev.*, **111**, 1998-2004.

Melack, J. M., L. L. Hess, and S. Sippel, 1994: Remote sensing of lakes and floodplains in the Amazon basin, *Remote Sensing Reviews*, **10**, 127-142.

Monson, R. K., M. T. Lerdau, T. D. Sharkey, D. S. Schimel, and R. Fall, 1995: Biological aspects of constructing volatile organic compound emission inventories, *Atmospheric Environment*, **29**, 2989-3002.

Morrissey, L. A., G. P. Livingston, and S. L. Durden, 1994: Use of SAR in regional methane exchange studies, *Int. J. of Remote Sensing*, **15**, 1337-1342.

Mosier, A., D. Schimel, D. Valentine, K. Bronson, and W. Parton, 1991: Methane and nitrous oxide fluxes in native, fertilized and cultivated grasslands, *Nature*, **350**, 330-332.

Myneni, R. B., S. Maggion, J. Iaquinta, J. L. Privette, N. Gobron, B. Pinty, D. S. Kimes, M. M. Verstraete, and D. L. Williams, 1995: Optical remote sensing of vegetation: modeling, caveats, and algorithms, *Remote Sens. Environ.*, **51**, 169-188.

Myneni, R. B., S. O. Los, and C. J. Tucker, 1996: Satellite-based identification of linked vegetation index and sea surface temperature anomaly areas from 1982-1990 for Africa, Australia and South America, *Geophys. Res. Lett.*, **23**, 729-732.

Parton, W. J., J. W. B. Stewart, and C. V. Cole, 1988: Dynamics of C, N, P, and S in grassland soils: A model, *Biogeochemistry*, **5**, 109-131.

Paul, E. A., and F. E. Clark, 1989: *Soil Microbiology and Biochemistry*, 273 pp.

Philander, S. G. H., 1986: Unusual conditions in the tropical Atlantic ocean in 1984, *Nature*, **322**, 236-238.

Philander, S. G. H., 1990: El Niño, La Niña, and the Southern Oscillation, International Geophysics Series, **46**, 293.

Pope, K. O., J. M. Rey-Benayas, and J. F. Paris, 1994: Radar remote sensing of forest and wetland ecosystems in the Central American tropics, *Remote Sens. Environ.*, **48**, 205-219.

Pope, K. O., E. J. Sheffner, K. J. Linthicum, C. L. Bailey, T. M. Logan, E. S. Kasischke, K. Birney, A. R. Njogu, and C. R. Roberts, 1992: Identification of Central Kenyan Rift Valley fever virus vector habitats with Landsat TM and evaluation of their flooding status with airborne imaging radar, *Remote Sens. Environ.*, **40**, 185-196.

Potter, C. S., J. T. Randerson, C. B. Field, P. A. Matson, P. M. Vitousek, H. A. Mooney, and S. A. Klooster, 1993: Terrestrial ecosystem production: A process model based on global satellite and surface data, *Global Biogeochemical Cycles*, **7**, 811-841.

Prather, M., R. Derwent, D. Ehhalt, P. Fraser, E. Sanhueza, and X. Zhou, 1995: Other trace gases and atmospheric chemistry, in *Climate Change 1994: Radiative Forcing of Climate Change and An Evaluation of the IPCC IS92 Emission Scenarios*, (J. T. Houghton, L. G. Meira Filho, J. Bruce, H. Lee, B. A. Callander, E. Haites, N. Harris, and K. Maskell, Eds.), Cambridge University Press, Cambridge, UK, pp. 75-126.

Reichle Jr., H. G., V. S. Connors, J. A. Holland, W. D. Hypes, H. A. Wallio, J. C. Casas, B. B. Gormsen, M. S. Saylor, and W. D. Hesketh, 1986: Middle and upper tropospheric carbon monoxide mixing ratios as measured by a satellite-borne remote sensor during November 1981, *J. Geophys. Res.*, **91**, 10865-10887.

Reichle, H. G., V. S. Connors, J. A. Holland, R. T. Sherrill, H. A. Wallio, J. C. Casas, E. P. Condon, B. B. Gormsen, and W. Seiler, 1990: The distribution of middle tropospheric carbon monoxide during early October 1984, *J. Geophys. Res.*, **95**, 9845-9856.

Rodgers, C. D., 1976: Retrieval of atmospheric temperature and composition from remote measurements of thermal radiation, *Reviews of Geophysics and Space Physics*, **14**, 609-624.

Ropelewski, C. F., and M. S. Halpert, 1987: Global and regional scale precipitation patterns associated with the El Niño/Southern Oscillation, *Mon. Wea. Rev.*, **115**, 1606-1626.

Ropelewski, C. F., and M. S. Halpert, 1989: Precipitation patterns associated with the high index phase of the Southern Oscillation, *J. Climate*, **2**, 268-284.

Ruimy, A., B. Saugier, and G. Dedieu, 1994: Methodology for the estimation of terrestrial net primary production from remotely sensed data, *J. Geophys. Res.*, **99**, 5263-5283.

Schimel, D. S., B. H. Braswell, R. McKeown, D. S. Ojima, W. J. Parton, and W. Pulliam, 1996: Climate and nitrogen controls on the geography and time scales of terrestrial biogeochemical cycling, *Global Biogeochemical Cycles*, **10**, 677-692.

Schimel, D., I. G. Enting, M. Heimann, T. M. L. Wigley, D. Raynaud, D. Alves, and U. Siegenthaler, 1995: CO_2 and the carbon cycle, *Climate Change 1994: Radiative Forcing of Climate Change and An Evaluation of the IPCC IS92 Emission Scenarios*, (J. T. Houghton, L. G. Meira Filho, J. Bruce, H. Lee, B. A. Callander, E. Haites, N. Harris, and K. Maskell, Eds.), Cambridge University Press, Cambridge, UK, pp. 35-71.

Schimel, D. S., W. J. Parton, F. J. Adamsen, R. G. Woodmansee, R. L. Senft, and M. A. Stillwell, 1986: The role of cattle in the volatile loss of nitrogen from a shortgrass steppe, *Biogeochemistry*, **2**, 39-52.

Schimel, D., and E. Sulzman, 1995: Variability in the Earth climate system: Decadal and longer timescales, *Rev. Geophys.*, Supplement, U.S. National Report to International Union of Geodesy and Geophysics 1991-1994, 873-882.

Sellers, P. J., Y. Mintz, Y. C. Sud, and A. Dalcher, 1986: A simple biosphere model (SiB) for use within general circulation models, *J. Atmosp. Sci.*, **43**, 505-531.

Sellers, P. and D. Schimel, 1993: Remote sensing of the land biosphere and biogeochemistry in the EOS era: science priorities, methods and implementation—EOS land biosphere and biogeochemical cycles panels, *Global and Planetary Change*, **7**, 279-297.

Shine, K. P., Y. Fouquart, V. Ramaswamy, S. Solomon, J. Srinivasan, et al., 1995: Radiative forcing, in *Climate Change 1994: Radiative Forcing of Climate Change and An Evaluation of the IPCC IS92 Emission Scenarios*, (J. T. Houghton, L. G. Meira Filho, J. Bruce, H. Lee, B. A. Callander, E. Haites, N. Harris and K. Maskell, Eds.), Cambridge University Press, Cambridge, UK, pp. 163-203.

Siegenthaler, U., and J. L. Sarmiento, 1993: Atmospheric carbon dioxide and the ocean, *Nature*, **365**, 119-125.

Sippel, S. K., S. K. Hamilton, J. M. Melack, and B. Choudhury, 1994: Determination of inundation area in the Amazon River floodplain using the SMMR 37 GHz polarization difference, *Remote Sens. Environ.*, **48**, 70-76.

Skole, D. and C. Tucker, 1993: Tropical deforestation and habitat fragmentation in the Amazon: Satellite data from 1978 to 1988, *Science*, **260**, 1905-1910.

Tans, P. P., I. Y. Fung, and T. Takahashi, 1990: Observational constraints on the global atmospheric CO_2 budget, *Science*, **247**, 1431-1438.

Taylor, F. W., 1983: Pressure modulator radiometry, in *Spectroscopic Techniques, Vol. III*, Academic Press, San Diego, pp. 137-197.

Tucker, C. J., I. Y. Fung, C. D. Keeling, and R. H. Gammon, 1986: Relationship between atmospheric CO_2 variations and a satellite-derived vegetation index, *Nature*, **319**, 195-199.

Tucker, C. J., H. E. Dregne, and W. W. Newcomb, 1991: Expansion and contraction of the Sahara Desert from 1980 to 1990, *Science*, **253**, 299-1073.

Valentine, D. W., E. A. Holland, and D. S. Schimel, 1994: Ecosystem and physiological controls over methane production in northern wetlands, *J. Geophys. Res.*, **99**, 1563-1571.

VEMAP Members, 1995: Vegetation/ecosystem modeling and analysis project (VEMAP): Comparing biogeography and biogeochemistry models in a continental-scale study of terrestrial ecosystem responses to climate change and CO_2 doubling, *Global Biogeochemical Cycles*, **9**, 407-438.

Wang, M.-X., S. Xingjian, S. Renxing, R. Wassman, and W. Seiler, 1993: Methane production, emission and possible control measures in rice agriculture, *Advances in Atmospheric Sciences*, **10**, 307-314.

Wang, Y., S. Filoso, L. Hess, and J. M. Melack, 1995: Understanding the radar backscattering from flooded and nonflooded Amazonian forests: results from canopy modeling, *Remote Sens. Environ.*, **54**, 324-332.

Wong, C. S., Y.-H. Chan, J. S. Page, G. E. Smith, and R. D. Bellegay, 1993: Changes in equatorial CO_2 flux and new production estimated from CO_2 and nutrient levels in Pacific surface waters during the 1986/87 El Niño, *Tellus*, **45B**, 64-79.

Woodruff, S. D. et al., 1993: Comprehensive Ocean-Atmosphere Data Set (COADS). Release 1a, NOAA, Washington DC.

Yienger, J. J., and H. Levy II., 1995: Empirical model of global soil-biogenic NO_x emissions, *J. Geophys. Res.*, **100**, 11,447-11,464.

Chapter 4 Index